Precambrian Research 362 (2021) 106322

Contents lists available at ScienceDirect

Precambrian Research

journal homepage: www.elsevier.com/locate/precamres

Distributed crustal shortening followed by transpressional shearing in the Superior Province, northeastern Canada: A Late Archean analogy to modern accretionary plate margins?

Jiří Žák [a,*], Filip Tomek [a,b], Martin Svojtka [b], František Vacek [a,c], Václav Kachlík [a], Lukáš Ackerman [b], Josef Ježek [d], Michael S. Petronis [e]

[a] Institute of Geology and Paleontology, Faculty of Science, Charles University, Albertov 6, Prague 12843, Czech Republic
[b] Institute of Geology of the Czech Academy of Sciences, Rozvojová 269, Prague 16500, Czech Republic
[c] Czech Geological Survey, Klárov 3, Prague 11821, Czech Republic
[d] Institute of Applied Mathematics and Information Technologies, Faculty of Science, Charles University, Albertov 6, Prague 12843, Czech Republic
[e] Environmental Geology, Natural Resources Management Department, New Mexico Highlands University, Las Vegas, NM 87701, USA

ARTICLE INFO

Keywords:
Anisotropy of magnetic susceptibility (AMS)
Archean tectonics
Granite
Pluton
Superior Province
Syn-tectonic emplacement

ABSTRACT

The Canadian Superior Province has become one of the key test pieces to discuss tectonic processes and mechanisms of crustal growth in the Late Archean. The Province consists of a >2.8 Ga proto-cratonic core intruded by voluminous arc-like plutons and surrounded by a series of narrow, elongate ca. 2.8–2.7 Ga juvenile belts, also referred to as terranes or domains. The terranes seem to wrap around the proto-cratonic core and generally young outward, but the kinematics and geodynamic causes of their assembly remain debated. In this paper, we examine the Radisson pluton in northeastern Québec, which intruded the southern, outer edge of the presumed magmatic arc (Bienville domain) along its ~WNW–ESE-trending tectonic boundary with the proto-cratonic crust (La Grande domain). The pluton, dominated by porphyritic monzogranite to quartz monzonite, was emplaced at around 2712 Ma and exhibits complex internal structure resulting from superposed magmatic to solid-state deformations. An early margin-parallel ~WNW–ESE magmatic foliation containing a steep lineation, recognized by the anisotropy of magnetic susceptibility (AMS), is interpreted as recording vertical stretching and horizontal flattening of highly crystallized magma, either due to emplacement and/or pure shear dominated transpression. More widespread, however, is a horizontal lineation within the same foliation that is interpreted as recording post-emplacement, but still syn-magmatic, tectonic strain (~NNE–SSW shortening and boundary-parallel stretching). Upon cooling, localized dextral S–C mylonite zones accommodated further shortening within the pluton whereas undeformed late-stage felsic dikes cross-cut the solid-state fabric at an angle to the pluton margins. We suggest that this structural succession, also reproduced by numerical fabric modeling, is a local-scale signal of a two-stage assembly of the northeastern Superior Province: the frontal, NNE-directed terrane convergence and attachment to the cratonic nucleus, operating in a 'hot' regime with voluminous arc-like plutonism, was followed by more localized dextral shearing parallel to terrane boundaries. The latter phase is recorded at the proto-craton margin but also in the outboard Abitibi greenstone belt virtually at the same time (ca. 2700–2690 Ma). In combination, the two-stage evolution and similar deformation distributed over a broad region resemble modern large hot orogens formed in a plate-tectonic regime.

1. Introduction

The transition from vertical, plume-dominated tectonics to modern-style plate motions has been debated extensively for decades (see, e.g., Kröner, 1985; Davies, 1992; de Wit, 1998; Hamilton, 1998a; Hamilton, 1998b; Cawood et al., 2006; Smithies et al., 2007; Stern, 2008; Ernst, 2009; Hamilton, 2011; van Hunen and Moyen, 2012; Korenaga, 2013; Arndt, 2013; Wyman, 2013; Gerya, 2014; Bédard, 2018; Condie, 2018; Brown and Johnson, 2018; Cawood et al., 2018; Moyen and Laurent, 2018; Brown et al., 2020; Stern, 2020; Windley et al., 2021; Palin and

* Corresponding author.
E-mail address: jirizak@natur.cuni.cz (J. Žák).

https://doi.org/10.1016/j.precamres.2021.106322
Received 9 April 2021; Received in revised form 6 July 2021; Accepted 9 July 2021
Available online 27 July 2021

Santosh, 2021 for overviews and discussions). In particular, the most intriguing issues include the timing of this transition and the onset of subduction of cold oceanic lithosphere and the derivation mechanisms of vast volumes of Archean tonalite–trondhjemite–granite (TTG) suite to generate the juvenile continental crust. Each issue has been framed by opposing end-member views: for the former, estimates for the age of onset of plate tectonics range widely from ca. 4.3 Ga to ca. 900–800 Ma (e.g., Stern, 2008; Harrison et al., 2008; Brown and Johnson, 2018; Xia et al., 2019), while for the latter some models prefer melting of thick, hydrated oceanic plateaus in favor of supra-subduction zone arc magmatism (see, e.g., Smithies, 2000; Condie, 2005; Smithies et al., 2009; Moyen, 2011; Moyen and Martin, 2012; Arndt, 2013; Martin et al., 2014; Palin et al., 2016; Johnson et al., 2017; Moyen and Laurent, 2018 for discussions).

As noted above, the Archean crust is volumetrically dominated by intermediate to felsic gneiss complexes and plutons that were often emplaced in a general temporal succession from the TTG association to high-K sanukitoids and 'hybrid' granitoids (e.g., Moyen et al., 2003; Martin et al., 2005; Martin et al., 2010; Laurent et al., 2014; Halla et al., 2017). As the petrogenetic and tectonic significance of their geochemical composition, i.e., whether they formed above mantle plumes or above subduction zones, remains a matter of dispute, it begs an

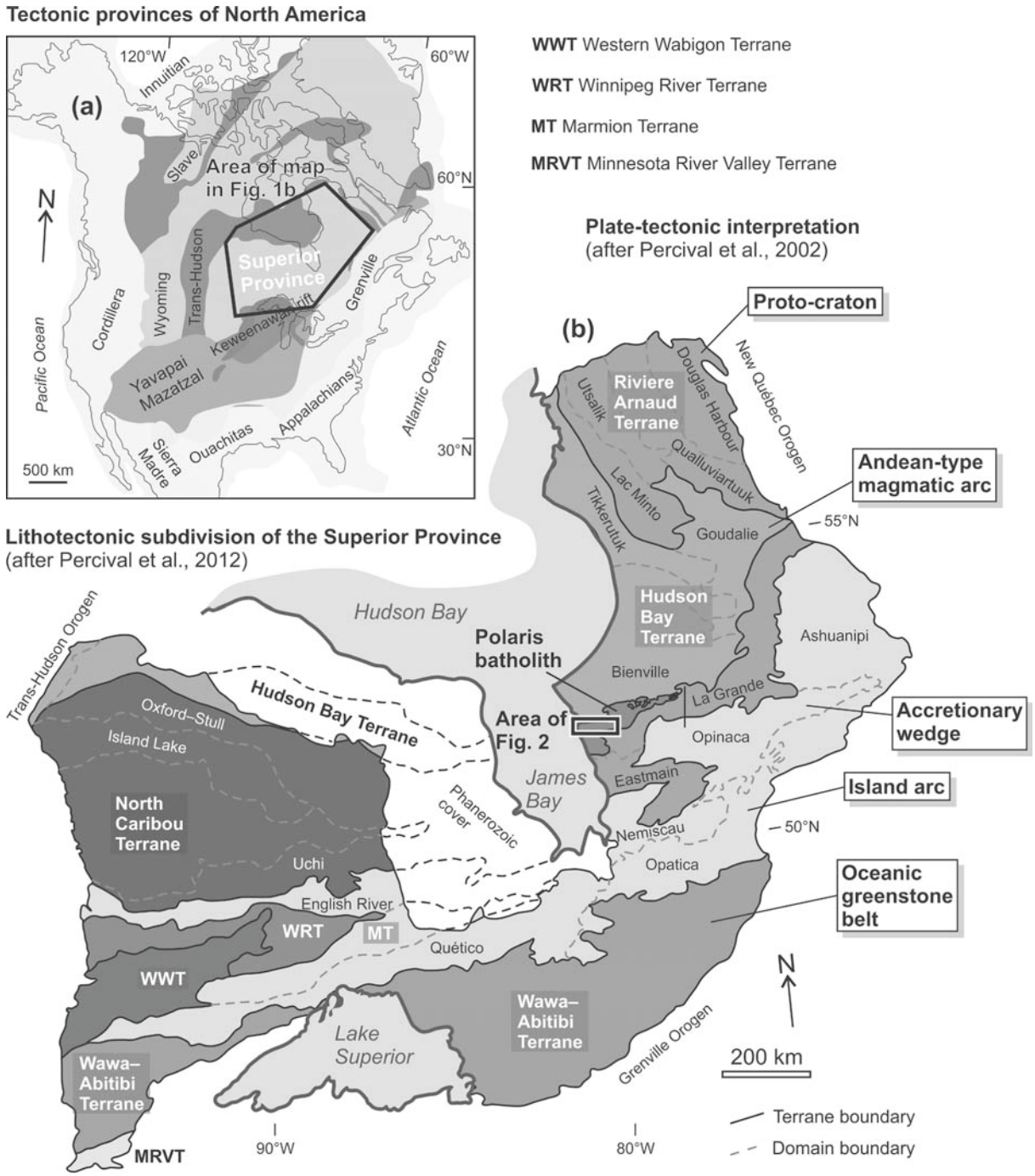

Fig. 1. Overview geologic map of the Superior Province, its principal terranes and domains, and their plate-tectonic interpretation (modified after Percival et al., 1994; Percival et al., 2012). Inset shows the position of the Province as a continental cratonic core of North America (simplified from Whitmeyer and Karlstrom, 2007).

outstanding question: are there any additional criteria that could help to resolve the issue?

Structural and fabric studies in Archean granitic terrains have highlighted the importance of analyzing crustal strain patterns for discriminating between the gravity-driven (diapiric) and tectonic-driven processes (e.g., Bouhallier et al., 1993; Chardon et al., 2002; Chardon et al., 2009). A fundamental change in intrusive geometries of Archean gneiss domes and plutons from ovoid to elongate in plan view is observed between 3.5 and 2.5 Ga, in conjunction with changes in the associated strain fields (e.g., Van Kranendonk et al., 2007; Cagnard et al., 2011). Although complexities resulting from the interplay between diapiric and tectonic processes do occur in Archean terrains (e.g., Bloem et al., 1997; Jelsma and Dirks, 2000), the former type of intrusions is typically associated with pluton-up/host rock-down kinematics, steep stretching lineations, and significant flattening of the host rock (e.g., Brun et al., 1981; Ramsay, 1989; Collins et al., 1998), whereas the latter is associated with strike-slip kinematics, horizontal lineations, and plane strain (e.g., Bouhallier et al., 1993; Pawley et al., 2002). The key role of regional tectonic deformation, and orogen-parallel shearing in particular, in controlling granitic magma ascent, emplacement, and syn- to post-emplacement deformation may thus aid in discriminating between the two end-member emplacement modes and tectonic styles in the Precambrian. Moreover, an extensive body of literature from Phanerozoic collisional orogens and magmatic arcs has demonstrated that granitic plutons are extremely sensitive crustal strain markers, as their internal fabrics are easily reset due to increments of tectonic strain during final magma crystallization (e.g., Benn, 1994; Fowler and Paterson, 1997; Paterson et al., 1998; Bouchez, 2000; Žák et al., 2008; Žák and Kabele, 2012; Tomek et al., 2017). In summary, the structural inventory of plutons, especially when combined with anisotropy of magnetic susceptibility (AMS), may provide the key constraints on large-scale tectonic processes (e.g., Benn et al., 1998; Benn et al., 2001; Archanjo et al., 2002; Ghalamghash et al., 2009; Žák et al., 2015; Žák et al., 2017; Burton-Johnson et al., 2019).

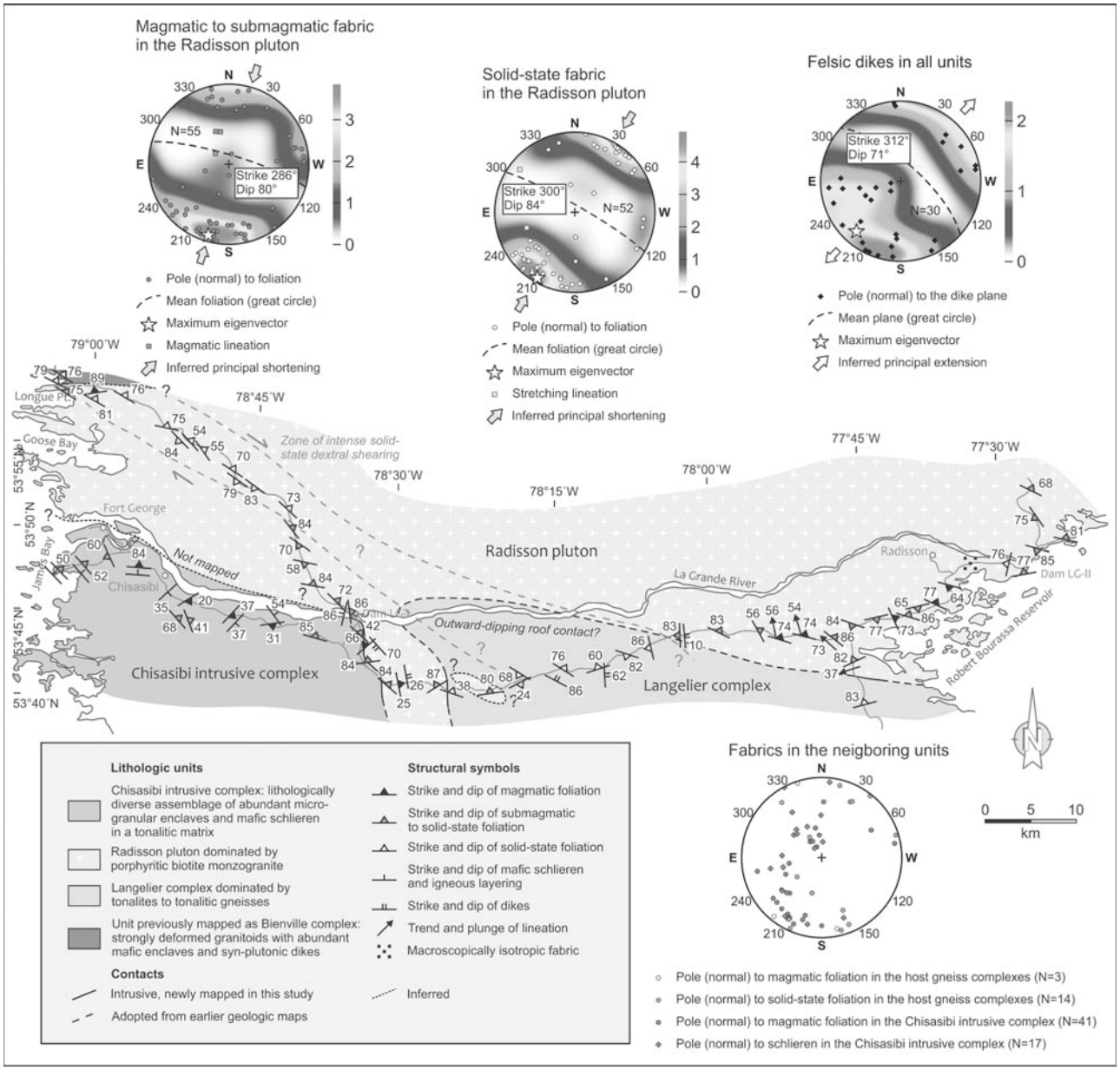

Fig. 2. Structural map showing orientation of magmatic to solid-state fabrics and other features (mafic schlieren, dikes) in the Radisson pluton and adjacent gneiss and intrusive complexes. Stereonets (equal area, lower hemisphere projection) show the orientation of structural elements. Radiometric age of the pluton taken from Mortensen and Ciesielski (1987), geology modified from SIGEOM (Système d'information géominière of Québec).

This paper examines in detail an illustrative example of a Late Archean granitic pluton emplaced along a major tectonic boundary in the Superior Province, northeastern Québec, Canada (Figs. 1, 2). To characterize the syn-magmatic strain patterns, we integrate structural and kinematic analysis with anisotropy of magnetic susceptibility (AMS) and numerical modeling of fabric development in response to strain increments. These data sets are then combined into a geological model and used as a basis for a general discussion on the significance of pluton fabrics, interfering intrusive and tectonic strains, and finally also on evaluating various scenarios for the Late Archean assembly of the Superior Province.

2. Geological setting

2.1. The Superior Province

The Superior Province underlies much of the central and northeastern Canada and north-central United States (Fig. 1). The internal architecture of the Province differs remarkably from that of Paleo- to Mesoarchean cratons, which are characterized by gneissic domes surrounded by mafic keels (e.g., Pilbara, Kaapvaal; De Wit et al., 1992; Van Kranendonk et al., 2007; Eriksson et al., 2009), in that it consists of a series of narrow, elongate belts in map view. This feature makes it similar to younger cratons assembled during the Neoarchean, such as the Yilgarn craton in Western Australia (e.g., Myers, 1993; Czarnota et al., 2010; Zibra, 2020).

The northeasterly portion of the Superior Province encloses variably reworked slivers of >3.0 Ga basement referred to as the 'Superior protocraton' whereas the southerly and southwesterly belts represent ca. 2.8–2.7 Ga juvenile crust (see, e.g., Gibb, 1975; Card and Ciesielski, 1986; Card, 1990; Williams, 1990; Sleep, 1992; Kimura et al., 1993; Percival et al., 1994; Calvert et al., 1995; Lucas and St-Onge, 1998; Calvert and Ludden, 1999; Percival et al., 2006; Percival, 2007; Percival et al., 2012; Wyman, 2013; Wyman, 2018 for details). The belts young generally from north to south and strike ~WNW–ESE in the northwest, ~WSW–ENE across much of the Province in the center and east, changing to ~N–S and ~NNW–SSE in the northeast (Fig. 1). This architecture was interpreted in terms of modern plate tectonics (Fig. 1): the Bienville and its correlative Tikkerutuk and Utsalik plutonic domains as Andean-type magmatic arcs (e.g., Stem et al., 1994; Percival et al., 1994; Percival et al., 2001), the Opinaca River–Nemiscau–Quetico metasedimentary belts as accretionary wedges (e.g., Percival, 1989; Davis et al., 1990; Fralick et al., 1992; cf. Cleven et al., 2020), and the volcano-plutonic belts (e.g., Opatica) as outboard island arc terranes bounded by thrust systems (e.g., Sawyer and Benn, 1993). The most studied Wawa–Abitibi greenstone belt (Fig. 1) was interpreted as recording impingement of a mantle plume into an intra-oceanic subduction zone–arc system (e.g., Polat et al., 1998; Polat and Kerrich, 1999; Wyman et al., 2002; Rehm et al., 2021). The plate-tectonic interpretation of the Superior Province was further supported by the Lithoprobe transect that revealed north-dipping reflectors beneath the belts, compatible with fossil subduction zones (e.g., Calvert et al., 1995; Percival et al., 2006; Cook et al., 2012). Moreover, van der Voo (2004), based on Percival et al. (1994), reinterpreted the >90° curvature of the outboard belts (terranes) from NNW–SSE to WNW–ESE around the inboard 'Minto block' as resulting from oroclinal bending as in modern orogenic belts (e.g., Johnston et al., 2013).

Though the plate-tectonic scenarios have been widely accepted, alternative models for the Superior Province also exist (e.g., Bédard et al., 2003; Bédard, 2006; Bédard, 2018). For instance, Bédard and Harris (2014) explained the architecture of the Province as resulting from disintegration of the cratonic lithosphere into separate continental ribbons by a mantle plume, followed by their collisions (subcretion) and craton re-assembly driven by horizontal flow and traction of the underlying mantle. Similarly, Cleven et al. (2020) interpreted the Opinaca belt as representing an extensional basin sourced from areas uplifted due to mantle upwelling.

2.2. The Bienville domain

The Bienville domain forms the southern portion of the Hudson Bay terrane (Fig. 1; Percival et al., 2012). The domain is mainly composed of tonalite–trondhjemite–granodiorite–granite plutonic suites, including pyroxene-bearing granodiorites, that exhibit a variable degree of deformation and metamorphism from undeformed to foliated gneisses. In some places, the plutons enclose screens of metasedimentary (of graywacke and conglomerate protolith) and metavolcanic (mafic) rocks, the latter being locally interstratified with banded iron formations. The Nd model ages, some of which are as old as 3.36 Ga, suggest that the plutonic suites were built on older cratonic basement (Percival et al., 2012). Although scarce, the reported U–Pb zircon ages are as old as 2820 Ma, but most are younger and point to the main magmatic pulses at 2745, 2725, 2712, and 2685 Ma (Percival et al., 2001). Tonalitic gneisses near the southern margin of the domain were dated at 2813.0 ± 7.4 Ma and 2811.4 ± 2.4 Ma while the 'Bienville gneiss' farther north yielded poorly constrained ages of 2819 + 170/−80 Ma and 2797 + 122/−80 (U–Pb on zircon; Mortensen and Ciesielski, 1987). Various bodies of biotite ± hornblende ± clinopyroxene granodiorite and biotite granite were then dated at 2725 ± 6 Ma, 2702 ± 8 Ma, 2698 ± 6 Ma, and 2679 ± 14 Ma (U–Pb on zircon; Percival et al., 2001).

3. The Radisson pluton and its host rocks

In this study, we examine in detail the southern margin of the Bienville domain along its contact with the La Grande subprovince (Figs. 1, 2). On a large scale, the Bienville–La Grande boundary was intruded by a suite of high-K sanukitoids ranging in composition from monzogabbro through biotite–hornblende monzodiorite, amphibole–biotite, and biotite quartz monzonite to most fractionated biotite (monzo)granite, collectively mapped as the Polaris batholith. In map view, the 265 × 65 km batholith is irregular and asymmetrically curved, involving four segments (Fig. 1). A wide NNW–SSE-trending segment in the west passes into a narrow, straight, WNW–ESE-oriented part, then again into an easterly, wide, and NNW–SSE-oriented segment that passes into an eastward-tapered WNW–ESE-trending end (Fig. 1).

The southwestern portion of the Polaris batholith is occupied by the Radisson pluton (Fig. 2; sensu Mercier-Langevin et al., 2012). The pluton makes up the narrow central batholith segment trending WNW–ESE and is well exposed from one host rock contact to another to the north and east of the village of Chisasibi (Fig. 2). The northern host rock was previously mapped as the ca. 2800 Ma Bienville gneiss complex (Mortensen and Ciesielski, 1987), but is poorly explored in this part, consisting of lithologically heterogeneous and in most places strongly deformed assemblage of mingled mafic and felsic intrusions. The southeastern host rock is lithologically uniform, comprised of typical TTG 'gray gneisses' of the La Grande subprovince (ca. 2800 Ma Langelier complex; Mortensen and Ciesielski, 1987). The pluton/host rock contacts are intrusive, typically sharp-planar, but locally may also be sheeted with thin granitic sheets intruding along foliation planes in gneisses or preserved as thin host rock screens within the pluton. The contacts trend generally WNW–ESE, but in detail may be curved in plan view, taking abrupt, nearly 90° bends (Fig. 2). Based on field observations and aeromagnetic data, the northwestern contact may be steep while the southeastern contact may be flat or gently dipping to the south, away from the pluton (Fig. 2).

The bulk of the Radisson pluton is compositionally uniform, dominated by deformed, strongly porphyritic quartz monzonite with K-feldspar phenocrysts typically 2–3 cm in size set in a medium-grained matrix. Other minor lithologies include finer-grained equigranular monzodiorite to monzogabbro (in enclaves and syn-plutonic dikes) and dikes of pink biotite (monzo-)granite, aplite, and pegmatite.

The Polaris batholith has been dated by Mortensen and Ciesielski

(1987). The porphyritic granodiorite from a central part of the batholith yielded an age of 2712.0 + 3.2/−2.3 Ma (U–Pb on zircon), interpreted as a crystallization age. This age falls within a range of our unpublished U–Pb ages from the Radisson pluton (ca. 2719–2703 Ma).

4. Field observations and structural data

4.1. Host rock

In the northwesterly host rock, previously assigned to the Bienville gneiss complex (Mortensen and Ciesielski, 1987), foliation, schlieren, layering, and flattened enclaves dip, in general, at a steep angle to the ~NE (Fig. 2). In detail, however, the structures preserved here point to a complex magmatic–deformational history involving multiple magmatic pulses and magma mingling events that were penetratively overprinted by tectonic deformation. This polyphase history is evidenced by an earlier layering and mafic sheets boudinaged and then folded into tight to isoclinal folds with axial planes parallel to the dominant ~NW–SE steep foliation, which was intruded by late-stage pegmatitic dikes, which are, in turn, often folded and boudinaged (Fig. 3a–c). Meter-scale late-magmatic to solid-state ductile shear zones then cross-cut the foliation and layering. These shear zones are steep (80°–90°dip) and strike ~E–W.

To the south of the pluton, the tonalitic 'gray gneisses' of the Langelier complex (Figs. 2, 3d) exhibit fabrics ranging from magmatic in low-strain domains to widespread high-temperature solid-state fabrics (as defined using criteria outlined in Paterson et al., 1989; Paterson et al., 1998). The gneisses are composed of plagioclase (oligoclase to andesine), quartz, and dark green biotite, more mafic varieties may contain dark green amphibole, plagioclase prevails over quartz, K-feldspar is absent. Magmatic minerals are variably recrystallized, magmatic biotite flakes are replaced by smaller aggregates of biotite intergrowing

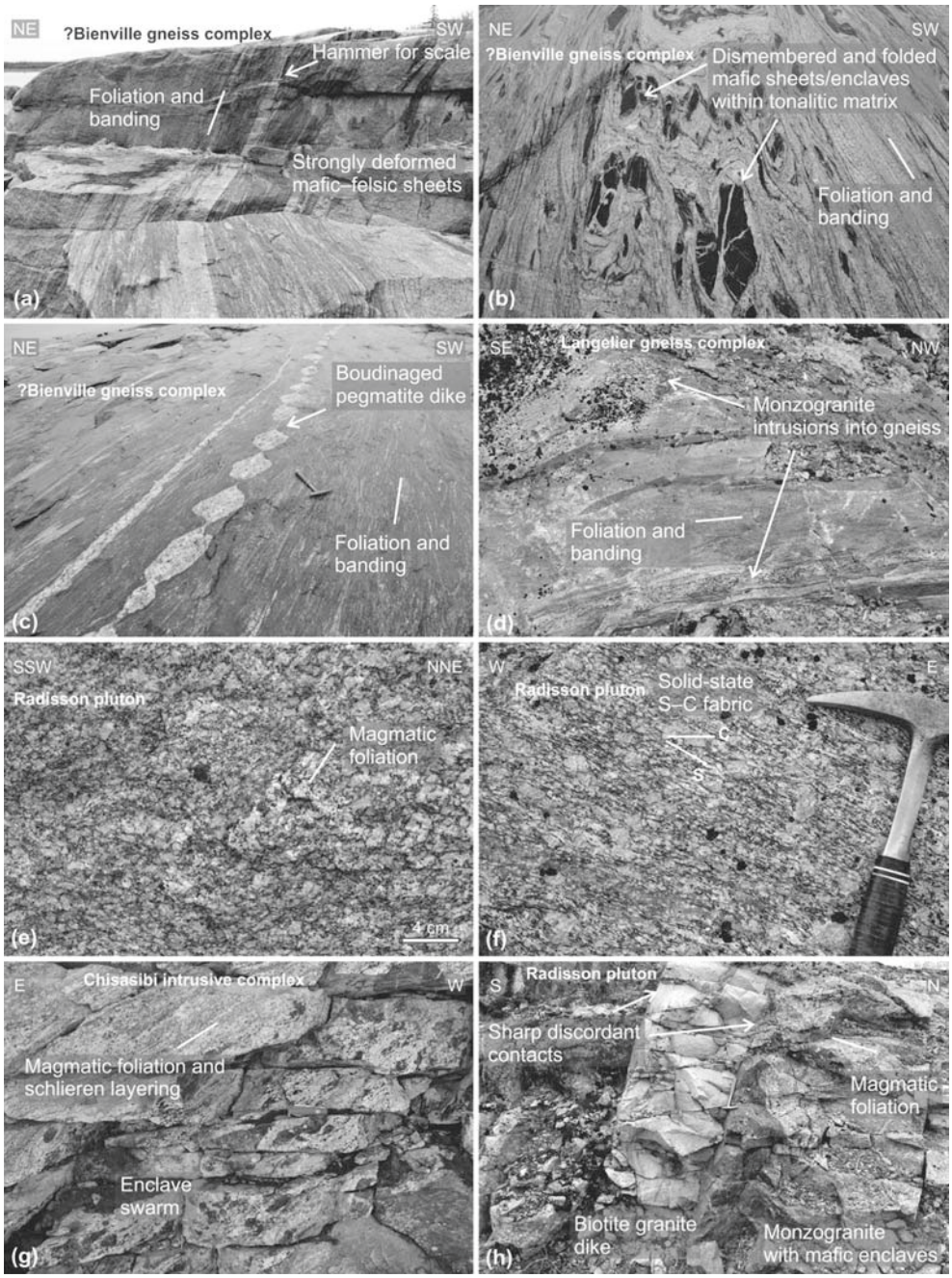

Fig. 3. Field examples of magmatic and solid-state structures in the Radisson pluton and adjacent intrusive complexes (GPS coordinates are referenced to the WGS84 datum). (a) Foliation and banding in structurally and lithologically complex unit to the north of the Radisson pluton, previously assigned to the Bienville domain. However, it cannot be excluded that this unit may belong to the younger magmatic cycle than is represented by the gneissic basement (question mark refers to this uncertainty), more geochemical and geochronological data are needed to solve this issue (GPS: 53.97405°N, 79.072817°W; hammer for scale, 31 cm in length). (b) Folded schlieren, banding, and mafic enclaves in the unit to the north of the Radisson pluton (GPS: 53.97405°N, 79.072817°W; Swiss Army knife for scale, 9 cm in length). (c) Boudinaged pegmatite dike that intruded along foliation planes, unit to the north of the Radisson pluton (GPS: 53.97405°N, 79.072817°W; hammer for scale, 31 cm in length). (d) Intrusive sheeted contact between the host Langelier gneiss complex and Radisson pluton (GPS: 53.659856°N, 78.423719°W; Swiss Army knife for scale, 9 cm in length). (e) Magmatic foliation is defined by K-feldspar phenocrysts, Radisson pluton (GPS: 53.7063°N, 78.566278°W). (f) Solid-state S–C fabric in the Radisson pluton (GPS: 53.906492°N, 78.797812°W; hammer for scale, 31 cm in length). (g) Shallowly-dipping schlieren and mafic enclaves in the Chisasibi intrusive complex (GPS: 53.754289°N, 78.847618°W; Swiss Army knife for scale, 9 cm in length). (h) Late-stage granite dike (dated at ~2696 Ma) cutting across microgranular enclaves, schlieren, and K-feldspar foliation in the host monzogranite (GPS: 53.7063°N, 78.566278°W; hammer for scale, 27 cm in length).

with Fe–Ti oxides, metamorphic anhedral titanite, and epidote. The solid-state fabric is macroscopically developed as prominent banding where dark, recrystallized biotite and biotite–hornblende bands alternate with quartzo-feldspathic bands on the millimeter to centimeter scale while planar mineral grain and aggregate alignment within bands define often anastomosing foliation that is parallel to the banding. The banding and foliation are steep while their strike varies but is predominantly ~NW–SE (Fig. 2).

4.2. Magmatic to solid-state fabrics in the Radisson pluton

A transition from magmatic to solid-state fabrics is preserved in the Radisson pluton. Magmatic fabric is mostly defined by the planar (foliation) and linear (lineation) shape-preferred orientation of euhedral to subhedral K-feldspar (perthitic microcline) phenocrysts and biotite and amphibole grains and aggregates in the surrounding matrix (Fig. 3e). A rare flat-lying foliation occurs near the southern margin of the pluton, presumably parallel to a gently-dipping contact and intrusive sheets into the host tonalitic gneiss (Fig. 2). At the northwestern pluton margin, magmatic foliation strikes roughly E–W and is also parallel to the pluton/host rock contact (Fig. 2). Otherwise, the magmatic foliation is steep in most cases (70°–90° dip) and strikes ~WNW or ~ESE (Fig. 2). The magmatic lineation was difficult to discern at most outcrops due to the lack of exposed suitable planes (foliation-parallel joints), where observed, the lineation plunges moderately to steeply to the ~NW and ~NNW (Fig. 2).

The magmatic fabric grades into a solid-state fabric that is widespread along the examined western transect across the pluton (Fig. 3f). The solid-state fabric is marked by ductile deformation of the K-feldspar phenocrysts into σ-type porphyroclasts (e.g., Passchier and Simpson, 1986), as well as ductile deformation of the matrix (stretched biotite and quartz aggregates), and S–C fabric (e.g., Berthé et al., 1979; Lister and Snoke, 1984; Gapais, 1989) was also found in many places. The solid-state foliation is steep and strikes generally ~NW–SE, at an angle to the pluton margin (Fig. 2). At outcrops, kinematic indicators such as K-feldspar phenocryst tiling, obliquity between subfabrics, and S–C relationships indicate predominantly dextral sense of shear (Fig. 3f).

4.3. The Chisasibi intrusive complex

Our new mapping revealed that the southwestern part of the Polaris batholith, previously undivided, comprises a plutonic unit lithologically distinct from the Radisson pluton. This lithologically and structurally varied plutonic unit comprises widespread mafic microgranular enclaves of monzogabbro to monzodiorite composition, mafic schlieren, igneous layering, and variably dismembered syn-plutonic dikes that are set in a coarse-grained monzonitic to (monzo-)granitic matrix (Fig. 3g) and frequently cross-cut by younger felsic dikes, ranging in composition from quartz monzonite through granite to fractionated granitic pegmatites and aplites. All lithologies typically contain perthitic microcline. This unit is provisionally referred to as the Chisasibi intrusive complex in this paper (U–Pb age estimated at ca. 2697 Ma; unpublished data).

The complex exhibits a magmatic foliation (defined by the planar shape-preferred orientation of dark green biotite and dark brown–green hornblende grains and aggregates and by mafic microgranular enclaves) and foliation-parallel mafic schlieren that dip gently to moderately to the ~SE and ~S (Figs. 2, 3g) and reorient into steep, ~NW–SE-trending submagmatic to high-temperature solid-state fabric (magmatic hornblende is replaced by blue-green metamorphic hornblende, biotite is recrystallized and replaced along cleavage planes by chlorite). This transition is expressed on the stereonet as a girdle about a ~NW–SE-trending axis (Fig. 2).

4.4. Late-stage minor intrusions

A variety of minor late-stage intrusions cross-cut the three units described above. These intrusions are mostly felsic in composition ranging from microgranite through aplite to pegmatite, but also include K-feldspar cumulates. The late-stage intrusions are particularly common in the Chisasibi complex. Here, they vary from larger (several meters across) irregular diapir-like blobs, which appear to deform the schlieren-rich host, to complex networks of thin dikes, some of which are folded while others are planar and truncate the host foliation. The K-feldspar cumulate intrusions are found in several places and vary from thin sheets concordant with the host foliation to irregular discordant bodies that show evidence of ductile shortening after their emplacement. In the Radisson pluton, felsic dikes are also common and appear undeformed in terms of their geometry (Fig. 3h). They vary in orientation but statistically tend to align along a mean ~NW–SE trend (Fig. 2), similar to that of magmatic or solid-state foliation. The parallelism of dikes and foliation is, however, only apparent as they have mostly sharp-planar intrusive contacts (and internal fabric parallel to dike margins) that truncate the feldspar phenocryst foliation or mafic schlieren (Fig. 3h).

5. Microstructures

In the Radisson pluton, an analysis of 26 representative thin-sections, cut perpendicular to the mesoscopic foliation and parallel to lineation (if observed, XZ section), revealed two domains characterized by distinct microstructures (defined using criteria outlined in Paterson et al., 1989; Vernon, 2000). Both the eastern and western domains include coarse-grained porphyritic amphibole–biotite monzonite and biotite (±amphibole) quartz monzonite to monzogranite with euhedral to subhedral K-feldspar phenocrysts up to 5 cm in size. The coarse-grained quartzo-feldspathic matrix includes biotite dominating over hornblende, apatite, titanite, and microphenocrysts of opaque phases.

The eastern-domain granites are characterized by magmatic to submagmatic hypidiomorphic microstructure with euhedral to subhedral feldspar, subhedral biotite, and anhedral quartz grains (Fig. 4a, b). The quartz often indicates dynamic recrystallization features such as chessboard pattern and grain-boundary migration. Some feldspars are characterized by grain size reduction and secondary plagioclase growth. No apparent shape-preferred orientation of minerals or brittle microstructures were identified in the matrix.

In contrast, the western domain is indicative of submagmatic to high-temperature solid-state deformation (Fig. 4c, d). This is evidenced by a chessboard pattern, grain-boundary migration, and in places also subgrain rotation in quartz grains and aggregates. The K-feldspar phenocrysts are often corroded along their margins, yielding grain size reduction, are reoriented into foliation bands, and are sheared into S–C bands. Similar features are observed in plagioclase. Rarely, feldspar grains contain brittle fractures oriented perpendicular to foliation suggesting a transition from high- to moderate-temperature subsolidus deformation. Biotite and magnetite microphenocrysts fill the gaps along the reoriented feldspar phenocrysts and quartz, all defining the S–C fabric with the dominant dextral kinematics. Some biotite grains are decomposed into clusters of other micas and opaque phases.

6. Magnetic fabric

6.1. Background of the method in brief

The anisotropy of magnetic susceptibility (AMS) was used to complement the structural data and to characterize the rock fabric using quantitative parameters (see Hrouda, 1982; Tarling and Hrouda, 1993; Borradaile and Henry, 1997; Bouchez, 1997; Bouchez, 2000; Borradaile and Jackson, 2010 for reviews and principles of the method).

Magnetic susceptibility k is a second-rank tensor, which is described by a matrix $k = M/h$, where M $[A \times m^{-1}]$ is a vector of material magnetization, and h $[A \times m^{-1}]$ is a vector of the applied magnetic field (SI units are used throughout this paper). To quantify the magnetic fabrics parameters and orientations, the following parameters are used.

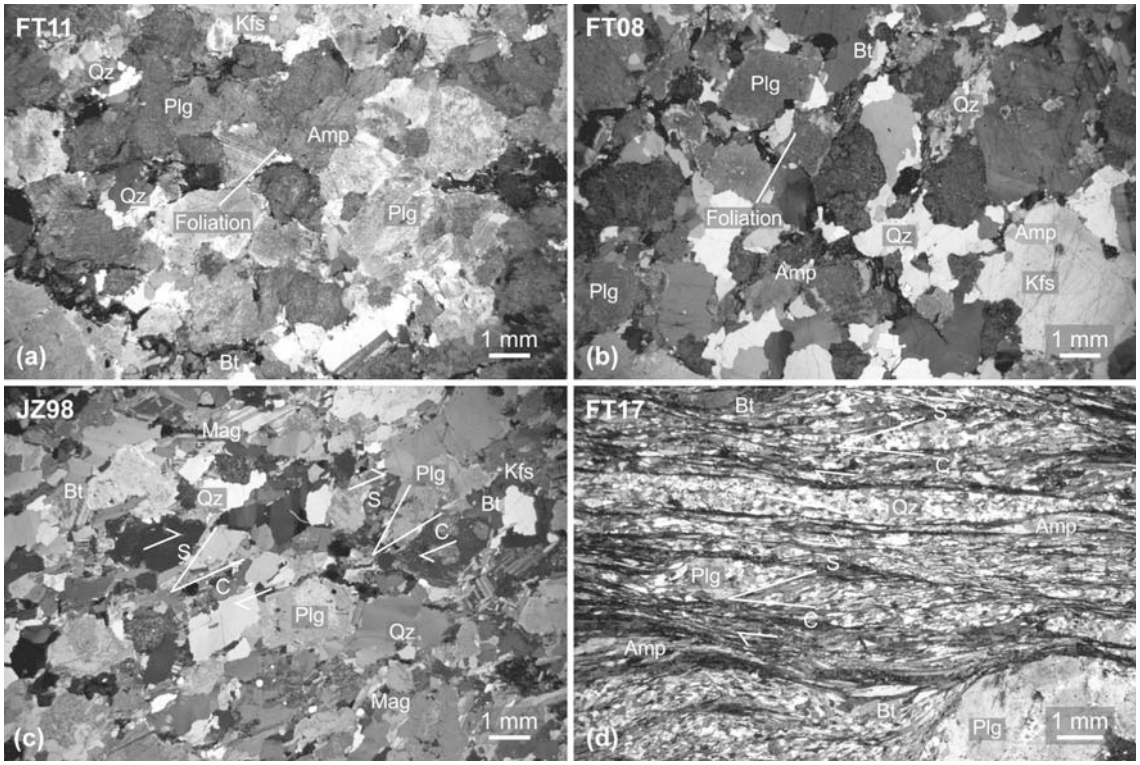

Fig. 4. Photomicrographs demonstrating a transition from magmatic through sub-magmatic to high-temperature solid-state microstructures and development of S–C fabrics in the Radisson pluton. (a) Weakly deformed and recrystallized cataclastic biotite–amphibole quartz monzonite with preserved magmatic fabric defined by preferred orientation of amphibole and plagioclase. Solid-state deformation and recrystallization is localized in matrix minerals (quartz and microcline). (b) Hypidiomorphic orthoclase and microcline and altered plagioclase phenocrysts together with recrystallized amphibole grains define magmatic foliation. Early crystallized hypidiomorphic to idiomorphic plagioclase shows magmatic compositional zoning with an albite rim at the contact with surrounding K-feldspar. In contrast, quartz grains are mostly dynamically recrystallized to fine-grained aggregates parallel to magmatic foliation. Microcline twinning, perthite, and myrmekite formed within high-strain zones of K-feldspar and prove strain passing from magmatic to sub-solidus conditions. (c) Biotite quartz monzonite showing partly recrystallized phenocrysts of both plagioclase and microcline and largely recrystallized matrix without significant grain-size reduction. Elongated feldspar phenocrysts define the S-planes, recrystallized biotite flakes are growing along S- and C-planes, are often bent around the feldspar phenocrysts, or occur in tails behind the preserved feldspar porphyroclasts. (d) Strongly sheared S–C type porphyroclastic amphibole–biotite quartz monzonite with relicts of partly recrystallized large (up to several cm) plagioclase and microcline and completely recrystallized ribbons of matrix minerals (biotite, amphibole, quartz, and feldspar) showing significant grain-size reduction. S-planes in ribbons are defined by flattening of recrystallized feldspar and quartz grains.

The maximum, intermediate, and minimum susceptibility axes are k_1, k_2, and k_3, respectively. The maximum principal susceptibility (k_1) represents the magnetic lineation and the minimum principal susceptibility (k_3) represents a normal to the magnetic foliation (k_1–k_2 plane). Hereinafter, three parameters are used to characterize the magnetic fabric: (1) the mean susceptibility, $k_m = (k_1 + k_2 + k_3)/3$, reflecting the magnetic mineral species and their proportion in the measured rock volume; (2) the degree of anisotropy, $P = k_1/k_3$, which expresses the eccentricity of the AMS ellipsoid; and (3) the shape parameter, $T = 2\ln(k_2/k_3)/\ln(k_1/k_3) - 1$, which describes the shape of the AMS ellipsoid; for $-1 \leq T < 0$ the ellipsoid is prolate, for $T = 0$ it is triaxial, and for $1 \geq T > 0$ it is oblate. The orientation of magnetic foliations and lineations is plotted in the lower hemisphere equal area stereographic projection and as the station mean directions on the map. The AMS parameters are visualized in the k_m–P and P–T diagrams. The orientation of magnetic fabrics is plotted in the stereographic equal-area projections on the lower hemisphere.

6.2. Sampling strategy and data acquisition

In this study, the samples for AMS were drilled in outcrops using a hand-held gasoline-powered drill at 40 stations along two transects across the Radisson pluton (28 stations) and adjacent parts of the Chisasibi intrusive complex (7 stations) and Langelier complex (5 stations). The western transect is a continuous profile from one pluton margin to another while the eastern transect represents only the southern margin of the wide segment of the pluton.

The AMS was measured using a MFK1-A Kappabridge equipped with a 3D rotator (Studýnka et al., 2014) in the Laboratory of Rock Magnetism, Institute of Geology and Paleontology, Charles University, Prague. A statistical analysis of the data was carried out using the ANISOFT software package (www.agico.com). The measured data and parameters are presented in Figs. 5–9 and listed in full in the Supplementary material (Parts 1–3) to this article.

6.3. Bulk susceptibility and thermomagnetic curves

Crucial for interpretation of fabric development is the identification of mineralogical controls on AMS, whether it is dominated by paramagnetic and/or ferromagnetic grains. The former typically have magnetocrystalline anisotropy (e.g., biotite), with the principal susceptibilities corresponding to the crystallographic axes, whereas the latter possess shape anisotropy (e.g., magnetite), with the longest grain axis corresponding to the maximum principal susceptibility and the shortest grain axis corresponding to the minimum principal susceptibility (e.g., Hrouda, 1982; Borradaile and Jackson, 2010). The contribution of paramagnetic and ferromagnetic grains in a specimen may be roughly estimated from the bulk susceptibility (e.g., Hrouda and Kahan, 1991).

The mean (bulk) susceptibility of the analyzed specimens was

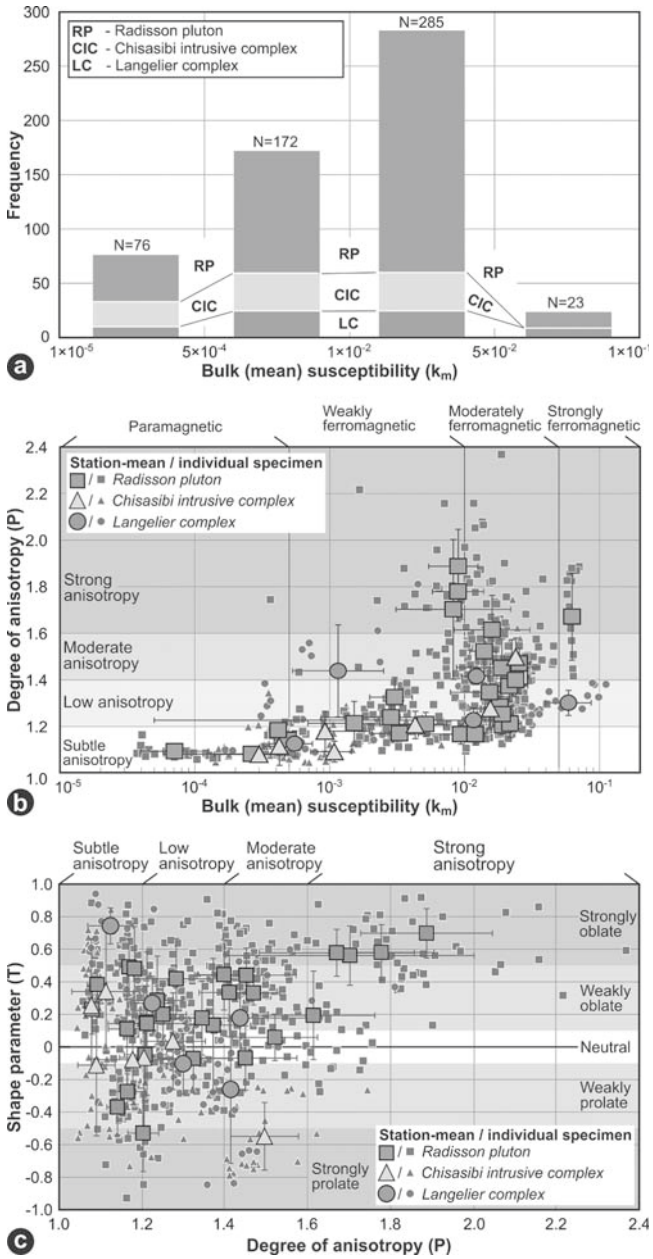

Fig. 5. Scalar parameters of all analyzed specimens in the sampled units. (a) Histogram of the bulk susceptibilities, (b) graph showing the relationship between the degree of anisotropy and bulk susceptibility, and (c) magnetic susceptibility P–T plot.

classified into four groups (Fig. 5a). Paramagnetic ($k_m < 5 \times 10^{-4}$SI), weakly ferromagnetic ($k_m = 5 \times 10^{-4} - 1 \times 10^{-2}$SI), moderately ferromagnetic ($k_m = 1 \times 10^{-2} - 5 \times 10^{-2}$SI), and strongly ferromagnetic ($k_m > 5 \times 10^{-2}$SI) values were measured in case of 14 % (6 stations), 31 % (14 stations), 51 % (18 stations), and 14 % (2 stations) of all the individual specimens, respectively (Fig. 5a). The Langelier gneiss complex is characterized only by ferromagnetic behavior; it includes 2 stations of weakly, 2 stations of moderately, and 1 station of strongly ferromagnetic susceptibility. The Radisson pluton yields 4 paramagnetic, 9 weakly, 14 moderately, and 1 strongly ferromagnetic value. The Chisasibi intrusive complex has overall lower susceptibilities represented by two paramagnetic, three weakly, and two moderately ferromagnetic stations.

To determine the AMS carriers more precisely, some additional analyses are required, in particular, the bulk susceptibility variation with temperature (see Hrouda, 1994; Hrouda et al., 1997 for theoretical background). This variation, plotted as thermomagnetic curves (Fig. 6a), was measured on 10 representative coarsely powdered specimens (7 specimens from the Radisson pluton, 2 specimens from the Chisasibi intrusive complex, and 1 specimen from the Langelier complex). The measurements were performed using the CS-L Cryostat and CS-4 Furnace instruments connected to an AGICO MFK1-A Kappabridge in the Laboratory of Rock Magnetism, Institute of Geology and Paleontology, Charles University, Prague. Complete thermomagnetic curves from –196 °C to 700 °C and back were obtained in three steps. First, the specimens were cooled down to the temperature of liquid nitrogen (ca. –196 °C) and heated to the room temperature (ca. 20 °C), magnetic susceptibility was measured approximately every minute. Second, the specimens were heated up in an argon atmosphere (to minimize mineral changes due to oxidation) from the room temperature to 700 °C and cooled back at an approximate rate of 14 °C/min. Third, the previously heated specimens were cooled down to –196 °C and heated to room temperature again. The data were statistically evaluated and plotted using the Cureval 8 software.

The paramagnetic group is described by a typical hyperbolic decrease of susceptibility from –197 °C up to 700 °C. The heating and cooling curves of sample JZ84 are fully reversible, whereas the cooling curve of sample JZ88 yields a Curie temperature (T_c) at ca. 578 °C; the cooling curve then follows a similar hyperbolic shape, however, at slightly higher susceptibility values implying growth of a new Fe–Ti oxide during the heating (Fig. 6b).

All the specimens from the ferromagnetic group display similar thermomagnetic curves (Fig. 6c–e) represented by an inferred, yet slightly elevated, Verwey transition (V_t) in the range of –152 °C and –145 °C, which is followed by a slight hyperbolic decrease to a room temperature and a linear increase in susceptibility with increasing temperature. An abrupt drop of susceptibility is recorded at Curie temperatures between 569 °C and 575 °C, which continues up to 700 °C. The cooling curves of samples follow a similar shape, while the susceptibility values of the cooling curves are slightly higher than that during heating (Fig. 6b, c, d). In addition, some specimens show a T_c around 623 °C (sample FT14), 645 °C (FT03), 655 °C (JZ97 and FT20), and 671 °C (FT09). Specimen FT03 has a slight bump of susceptibility on a heating curve at ca. 320 °C.

6.4. Hysteresis and FORC

We have shown that AMS is carried by magnetite grains in a large number of specimens (Fig. 5a, 6c–e). In case of magnetite, however, the fabric interpretation may not be as straightforward since very small, so-called single-domain magnetite grains exhibit an inverse magnetic anisotropy, i.e., their longest grain axis is not the maximum principal susceptibility (e.g., Potter and Stephenson, 1988). To exclude this phenomenon and to examine magnetic domain state, magnetic hysteresis and first-order reversal curves (FORC) were obtained from the Langelier gneiss complex (1 sample) and 7 samples from the Radisson pluton (see Roberts et al., 2000; Harrison et al., 2018 for theoretical background and Fig. 7a–c and 8a–c for idealized examples).

All hysteresis and first-order reversals curves (FORC) were collected with a Lake Shore Cryotronics Vibrating Sample Magnetometer Model 8600 at the New Mexico Highlands University Paleomagnetic-rock magnetic laboratory. Data collection used the MicroMag 2900/3900 software version 1.3 with a maximum applied field of 2.03 Tesla and field step size of 10 mT. The averaging time was 300 ms; data smoothing was minimum for all samples ($SF = 4$) given the high signal-to-noise ratio. Final processing of hysteresis loops was prepared in MS Excel and the FORC distribution was generated using the IgorPro Version 8.0.4.2 (WaveMetrics Inc) software. The number of first-order reversal curves varied between samples from 101 to 137 FORCs per sample to construct FORC distribution diagrams.

The room temperature hysteresis loops were acquired through the application of stepwise increasing uniaxial fields until the saturation is

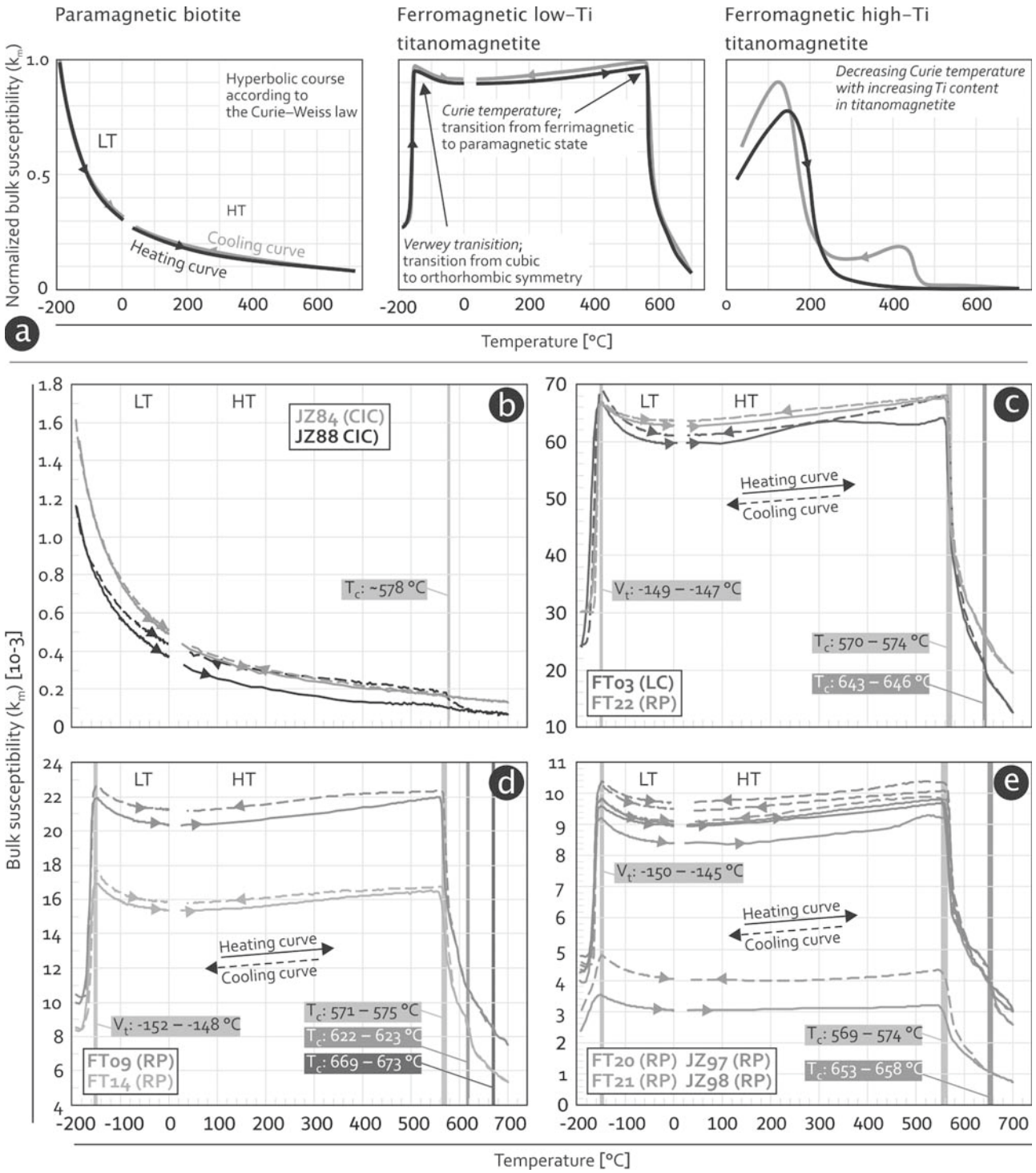

Fig. 6. Thermomagnetic curves. (a) Idealized thermomagnetic curves to illustrate different temperature–bulk susceptibility variations for paramagnetic and ferromagnetic minerals. (b–e) Measured thermomagnetic curves for selected specimens from the Chisasibi intrusive complex (CIC, panel b), Langelier complex (LC in panel c), and the Radisson pluton (RP in panels c, d, e).

reached. The experiments provide an important nondestructive tool for the investigation of the coercivity spectrum of the magnetic mineral(s) present within a sample (Fig. 7a–c). For magnetite, multi-domain (MD) grains are characterized by rapid acquisition and saturation at low applied fields while single-domain (SD) grains require a higher field to reach saturation. SD grains are said to be magnetically hard whereas MD grains tend to be magnetically soft. Hysteresis data provide information on both the dominant domain state of the magnetic fraction as well as the composition of the material. Magnetic hysteresis parameters (i.e., saturation remanent magnetization, M_r; saturation magnetization, M_s; and coercive force and coercivity of remanence, H_c and H_{cr}, respectively) provide information on both the dominant domain state of the magnetic fraction and the composition of the material.

Seven of the eight samples (both the Langelier complex and Radisson pluton) yield similar hysteresis loops characterized by steep acquisition and reach saturation between 0.25 T and 0.4 T with a saturation magnetization between 17 T and 225 T (average 82.5 T ± 82.1 T; 1σ; Fig. 7d). One sample (MS04; Radisson pluton) is distinct in that it does

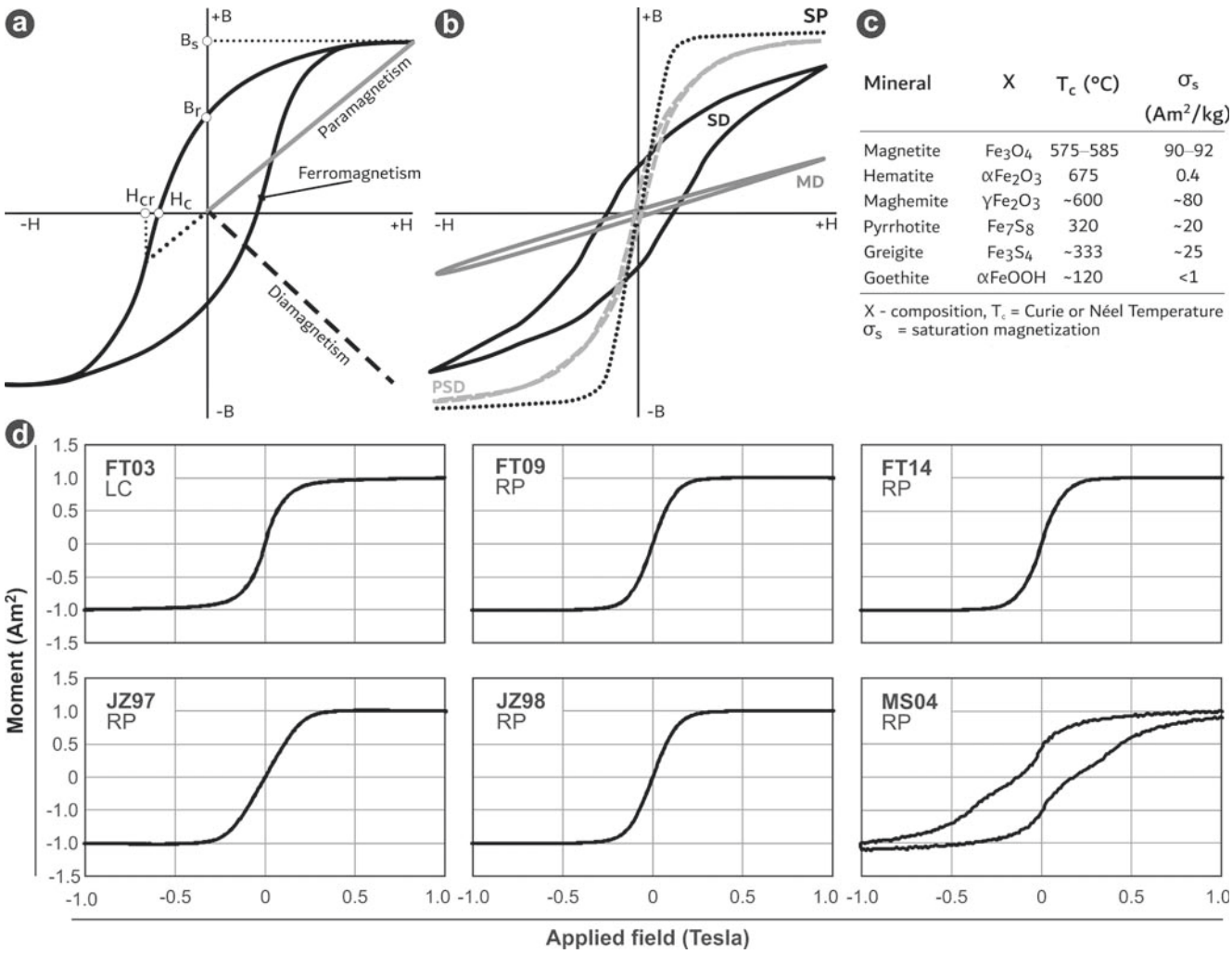

Fig. 7. Room-temperature hysteresis curves. (a) Ideal hysteresis curves showing magnetization behavior of diamagnetic, paramagnetic, and ferromagnetic (sensu lato (s.l.)) materials. Br, saturation remanent magnetization; Bs, saturation magnetization; Hc, coercive force, Hcr; coercivity of remanence; H, applied field; B (+/-), positive/negative induced magnetization (induction); H (+/-), positive/negative applied magnetic field. (b) Ideal hysteresis behavior for a ferromagnetic (s.l.) material of different domain states. SP, superparamagnetic; SD, single-domain; PSD, pseudosingle-domain (vortex state); MD, multi-domain. (c) Inset table: mineral, common ferromagnetic (s.l.) and antiferromagnetic mineral phases found in rocks; X, chemical formula of the mineral; σs, saturation magnetization (Am^2/kg) at room-temperature (modified from Dunlop and Özdemir, 1997). (d) Measured representative hysteresis loop diagrams of samples from the Langelier complex, LC (FT03) and Radisson pluton, RP (FT09, FT14, JZ98, JZ97, and MS04).

not reach saturation until ~1.6 T and yields a saturation magnetization of 0.23 T. The saturation magnetization values for the seven samples are consistent with a cubic phase of restricted composition likely titanomagnetite and/or titanomaghemite. The remaining sample with a low saturation magnetization reflects hematite and/or titanohematite as the principal magnetic phase.

A FORC is measured by saturating a sample in a field (H_{sat}) with a large positive magnetic field. The field is then decreased to a reversal field H_a and a partial hysteresis curve (a FORC) is measured as the applied field (H_b) increases from H_a back to saturation. This measurement procedure is repeated for a number of values of H_a to obtain a set of FORCs. The magnetization at the applied field H_b on the FORC with reversal point H_a is denoted by $M(H_a, H_b)$, where $H_b \geq H_a$. The FORC distribution is defined as the mixed second derivative: $\rho(H_a, H_b) = -\partial^2 M(H_a, H_b)/\partial H_a\, \partial H_b$. The FORC distribution $\rho(H_a, H_b)$ at a point P is calculated by fitting a polynomial surface $a_1 + a_2H_a + a_3H_a^2 + a_4H_b + a4H_b^2 + a_4H_aH_b$ on a local square grid centered at the point. The value $-a_6$ represents $r(H_a, H_b)$ at P. The smoothing factor (SF) defines the number of points $(2SF + 1)^2$ on the local grid used for the fitting. Smoothing reduces the effect of measurement noise magnified by taking the second derivative when calculating the FORC distribution. For plotting, the FORC distribution coordinates $\{H_a, H_b\}$ are conventionally rotated by 45° to $H_c = (H_b - H_a)/2$, $H_u = (H_b + H_a)/2$. A FORC diagram is a contour plot of a FORC distribution with H_u and H_c on the vertical and horizontal axes, respectively (Fig. 8a–c).

The measured six samples (FT03, FT09, FT14, FT21, FT22, JZ98) from the Langelier complex and Radisson pluton yield FORC distributions indicative of multi-domain grains (Fig. 8d), and two samples (JZ97, MS04; Radisson pluton) yield elongate distributions above and below the zero X-axis consistent with a mixture of domain states; likely multi-domain (MD) and pseudosingle-domain (PSD; Fig. 8d).

6.5. Magnetic fabric parameters

Though the degree of anisotropy (P) and shape parameter (T) vary widely as demonstrated in Fig. 5b, c, important trends can be seen from the eastern transect through the western transect to the Chisasibi complex (Fig. 9c). In this sequence, predominantly magmatic fabric in the eastern Radisson pluton yields a relatively lower degree of anisotropy with most data falling between 1.1 and 1.5 and both prolate and oblate shapes of the AMS ellipsoid whereas its western part with solid-state fabric yields higher P parameter and mostly oblate ellipsoids. Finally,

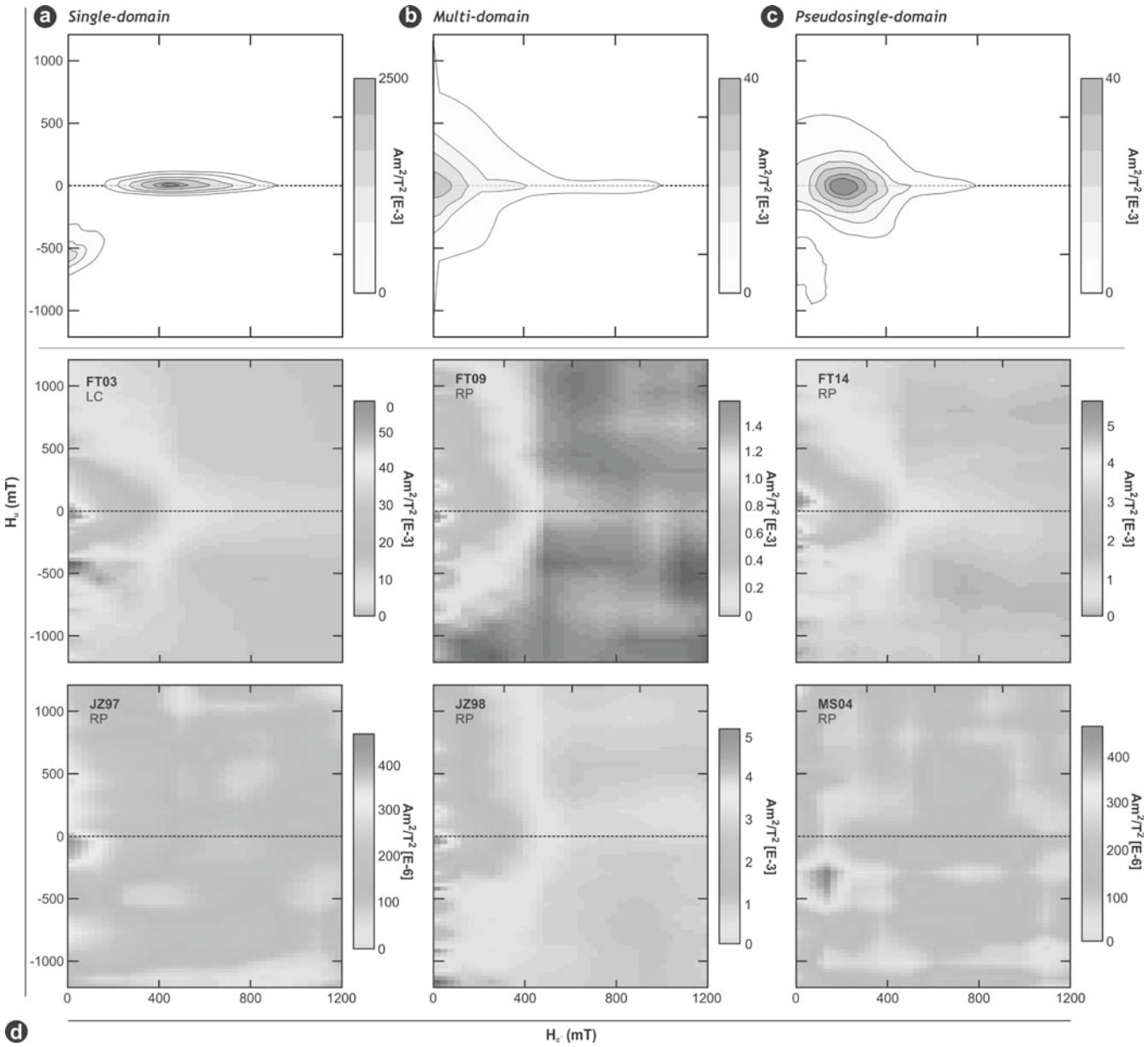

Fig. 8. Idealized First Order Reversal Curve (FORC) diagrams (a–c) for single-domain (SD), multi-domain (MD), and pseudosingle-domain (PSD) magnetite grains (modified from Harrison et al., 2018). The magnetic domain size for stable SD grains is between ~0.03 μm to ~0.08 μm, PSD grains are variable from >0.1 mm to 20 mm, and MD are larger than ~20 mm (Dunlop, 1973; Dunlop, 1995). However, the particle size range over which the transitions occur depends on many factors such as temperature, spontaneous magnetization, shape, and the state of internal stress of a particle (e.g., Day et al., 1977; Heider et al., 1987; Dunlop and Özdemir, 1997). Magnetite grains with different domain structures plot in different parts of the FORC distribution diagram. (a) Single-domain grains yield a narrow size-shape distribution with a single peak on the H_c (i.e., $H_u = 0$) axis. (b) Multi-domain grain sizes show a broad, vertically spread signal along the Hu direction with a weak, high-coercivity, horizontally spread tail perpendicular to the H_c axis (Pike et al., 2001). (c) Intermediate grain sizes of the pseudosingle-domain size (vortex state; Roberts et al., 2017) yield a well-defined closed-contour peak with a broad vertical and horizontal spreading along both H_c and H_u axis. (d) FORC distributions of samples from the Langelier complex, LC (FT03) and Radisson pluton, RP (FT09, FT14, JZ98, JZ97, and MS04). H_c coercive force; H applied field; H_a negative saturation applied field; H_b positive saturation applied field; $H_u = (H_a + H_b)/2$.

the Chisasibi complex shows a tendency towards prolate shapes of the AMS ellipsoid and again a lower degree of anisotropy (Fig. 9c). In map view, the shape of the AMS ellipsoid, as well as the degree of oblateness, vary irregularly across the sampled units, except at the western contact-to-contact transect in the Radisson pluton. Here, a strongly oblate fabric was measured at the northern pluton margin, weakly triaxial to weakly oblate in the center and again weakly oblate along the southern margin (Electronic Supplementary Material Part 3).

6.6. Magnetic fabric orientation

At most stations, the measured orientations of the principal susceptibility axes are well clustered, the site-mean directions are well defined, and the mean magnetic foliation corresponds well to the macroscopic, magmatic to solid-state mineral foliation (compare Fig. 2 with Fig. 9). Exceptions are stations FT06, FT11, JZ71, JZ82, and MS04 with magnetic and macroscopic foliations at a high angle to each other; these stations are interpreted with caution. In addition, stations FT25 and FT29 yield poorly clustered principal susceptibility axes; these stations

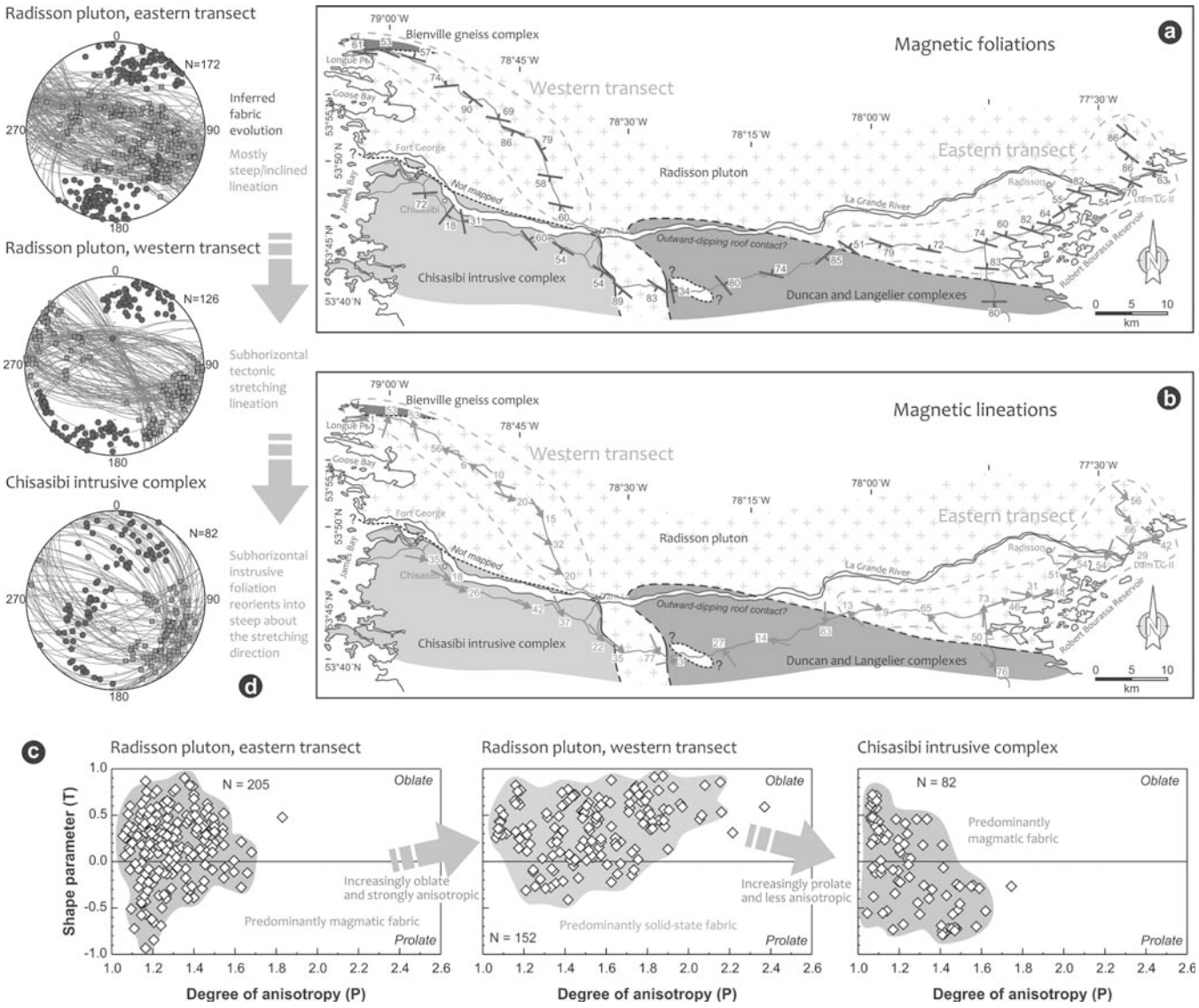

Fig. 9. Magnetic fabric in the Radisson pluton. Maps show orientation of (a) magnetic foliations and (b) magnetic lineations along two sampling transects. (c) Magnetic anisotropy P–T plots and (d) stereonets (lower hemisphere, equal area projection) indicate three stages of fabric evolution.

were excluded from further analysis.

Magnetic fabric orientation also exhibits a distinct trend similar to that of the scalar parameters described above. In the eastern transect of the Radisson pluton, magnetic foliation planes exhibit relatively homogeneous orientation and predominantly strikes ~WNW–ESE with a steep to moderate dip (two opposite clusters of data points on a stereonet; Fig. 9a, b, d). Magnetic lineations plunge steeply to moderately, variably scattered along the ~WNW–ESE foliation planes (Fig. 9b, d). In the western transect, magnetic foliation planes strike ~WNW–ESE near the pluton margins but also ~NW–SE in the pluton center and magnetic lineations plunge shallowly and trend ~WNW–ESE to ~NW–SE (Fig. 9a, b, d). A different pattern is observed in the Chisasibi complex, where magnetic foliation planes dip steeply to shallowly about a 'common' SE-plunging magnetic lineation (Fig. 9a, b, d).

7. Discussion

7.1. Tectonomagmatic history of the Bienville–La Grande boundary

Field relationships together with the existing geochronologic data indicate that multiple magmatic pulses intruded along the Bienville–La Grande boundary at different times and over a protracted time span. The punctuated but long-lasting plutonism evolved compositionally as in other Archean terrains, from the TTG suite, represented by the Bienville and Langelier gneisses, through the porphyritic monzonites and monzogranites of the Radisson pluton to heterogeneous, mingled mafic–felsic pulses of the Chisasibi complex to the late stage, minor felsic intrusions (see, e.g., Martin et al., 2010; Laurent et al., 2014 for a general discussion).

The oldest phase is represented by the emplacement of the Langelier gneiss complex at ca. 2800 Ma, likely a part of a voluminous and widespread event that formed the TTG proto-cratonic basement underlying much of the northeastern Superior Province (e.g., Percival et al., 1994). Unfortunately, this stage left no direct structural record in the Chisassibi–Radisson area due to the pervasive overprint under subsolidus conditions.

The dominant, regionally most widespread deformational structure is represented by the ~WNW–ESE steep foliation, which was found in the Bienville and Langelier gneiss complexes and also in the Radisson pluton (Fig. 2). While it is preserved as a solid-state feature in the former two units, the Radisson pluton exhibits a transition from magmatic and submagmatic fabric to high-temperature solid-state S–C mylonites

(Figs. 2, 3e, f, 4). Altogether this is an example of a coupled fabric pattern of Paterson et al. (1998) and, in turn, the Radisson pluton is interpreted as a *syn*-tectonic intrusion where deformation was coeval with its emplacement and cooling. As this deformational phase appears to affect a broad area along the Bienville–La Grande boundary and is an essential component in further interpretations, it is dealt with in considerable detail below.

7.2. Interpretation of pluton fabrics

Structural studies in syn-tectonic plutons have concluded that magmatic foliations and lineations record strain increments during final magma crystallization (e.g., Paterson and Vernon, 1995; Paterson and Miller, 1998; Paterson et al., 1998), with magmatic foliation representing the plane normal to the principal shortening (the Z-axis of the local strain ellipsoid) and magmatic lineation representing the principal stretching (the X-axis). The steep ~WNW–ESE magmatic foliation thus records protracted ~NNE–SSW horizontal shortening along the Bienville–La Grande boundary. At a map scale, though not constrained by structural data, the fold-like shape of the Polaris batholith is also at least compatible with the same regional shortening direction (Fig. 1).

The stretching axis (lineation) may be often difficult to retrieve from granite outcrops, the Radisson pluton being no exception. Yet, with the aid of rock-magnetic analyses suggesting the pseudosingle-domain (PSD) to multi-domain (MD) titanomagnetite as the main carrier of the AMS signal (Sections 6.3 and 6.4; Figs. 7, 8), we revealed two magnetic lineations in the pluton (Fig. 9b, d). Before discussing their significance further, it is important to note that we found no evidence for the presence of late-stage or secondary Fe–Ti phases that would either mimic the already established silicate mineral network or define new magnetic fabric. Such phases often occur as clustered aggregates of secondary minerals, e.g., new biotite, chlorite (chamosite), and secondary hornblende along with various Fe–Ti opaque phases. Instead, we observe primary magmatic hornblende, biotite, and magnetite microphenocrysts (Fig. 4a, b). This observation is further supported by our magneto-mineralogical analyses. The susceptibility-dominating phase across most of the studied samples from the Radisson pluton is the low-Ti titanomagnetite (see the uniform shape of thermomagnetic curves and Curie point temperatures; Fig. 6c–e) with only indistinct contribution of maghemite and hematite. In case of a late stage fluid flow, we would expect a non-uniform behavior of magnetic susceptibility (with different dominant mineral carriers) across such a large-scale pluton. Instead, here we report no mineralogical changes from pluton contact towards the pluton interior and uniform AMS carriers. Therefore, we argue that there is no late-stage hydrothermal fabric overprint in our samples.

The moderately to steeply plunging (>50°) lineations have been preserved in domains without pervasive solid-state overprint and are associated with oblate AMS ellipsoids, regardless of whether carried by ferromagnetic or paramagnetic minerals. These lineations could be interpreted in terms of either intrusive strain, recording vertical magma stretching along intrusion margins during emplacement (e.g., Cruden, 1990; Hrouda et al., 1999), or pure shear-dominated syn-magmatic transpression (e.g., Tikoff and Greene, 1997). The distinction between these two cases (intrusive vs. tectonic fabric) is generally difficult, especially in elongated syn-tectonic arc plutons, where intrusion margins are parallel to the trend of tectonic structures (foliations, folds, faults) in the host rock.

Furthermore, most of the AMS sites yield subhorizontal ~WNW–ESE magnetic lineations while the foliation remains steep; magnetic lineations thus plot along a great circle on a stereonet (Fig. 9b, d). This feature could be explained by a rotation of the principal shortening axis that would decrease its angle to the pluton margin and cause a switch from pure shear- to simple shear-dominated transpression. In simple shear-dominated transpression, the principal stretching axis is horizontal (e.g., Tikoff and Greene, 1997; Teyssier and Tikoff, 1999; Benn et al., 2001). However, evidence of a simple shear component at the magmatic to submagmatic stage is lacking on most outcrops. Asymmetric structures are rare, show no regionally consistent shear sense, and foliation is margin-parallel rather than margin-oblique or deflected as typical of shear zones. The key point in resolving this conundrum is whether horizontal stretching lineations may form in pure-shear dominated regimes. Most of the theoretical models of transpression prescribe the deforming zone as having a fixed bottom and free upper boundary to allow thickening (e.g., Sanderson and Marchini, 1984; Dutton, 1997; Schulmann et al., 2003), however, the boundary conditions in nature may be fundamentally different. Therefore, we employ numerical modeling (next section and Fig. 10) to examine fabric development in a deforming zone that is confined from above, for instance by a pluton roof or a rigid upper-crustal lid. The question is whether the laterally stretched magma mush will produce a horizontal lineation under such boundary conditions.

7.3. Numerical model of fabric evolution

The AMS data are suggestive of a steep lineation being reoriented to horizontal within a common, 'average' WSW–ENE-trending foliation plane (Fig. 9d). To test this idea, we performed numerical simulation using the mathematical approach and software developed by Ježek and Hrouda (2000, 2002). This method allows modeling the development of magnetic fabric (magnetic lineation and foliation and the parameters P and T) produced by an ensemble of magnetic particles embedded in a progressively deforming matrix in which they rotate as active or passive markers. It is therefore possible to search for strain history that is consistent with the observed AMS data.

In the model, presented in Fig. 10, we simulate the development of representative ('average') fabric in the Radisson pluton. We assume that the modeled features will apply with some variability to individual locations, i.e., the local initial fabric can be steeper or shallower and the fabric by the end of tectonic development varies around the modeled trend.

The initial fabric (Fig. 10a) represented by an 'average' fabric from the eastern transect (Fig. 9d), was approximated as a pre-oriented multiparticle system (the black dots in Fig. 10a are long axes of prolate magnetite grains with intrinsic susceptibility $k_i = 3$, grain degree of anisotropy $P = 1.76$, and aspect ratio $r = 3$). The calculated magnetic lineation plunges steeply (64°) to the ESE (the red square in Fig. 10a) and magnetic foliation is vertical, oriented WNW–ESE (pole to foliation is the blue dot in Fig. 10a).

In the second step (Fig. 10b), we simulate overprinting this initial fabric by pure shear regional deformation after magma emplacement but before its solidification. The pure shear (plane-strain) regime is modeled as horizontal shortening along the NNE–SSW direction to comply with the orientation of the measured foliations (Figs. 2, 9a). The upward motion of the deforming magma was confined, assuming there was an overlying rigid lid (pluton roof) above the present-day level of erosion. In the model, the progressive deformation leads to a significant shallowing of the magnetic lineation up to a plunge of 22° to the ESE (represented by the red square in Fig. 10b) while magnetic foliation remains virtually the same. The degree of anisotropy P increases and the symmetry of magnetic fabric T shifts towards a more oblate shape, fitting well magnetic fabric parameters measured in the western transect of the pluton.

In the third step (Fig. 10c), the previously produced fabric was superposed by progressive dextral simple shear along the NW–SE shear plane, in agreement with the measured field and AMS data from the western transect (Figs. 2, 9a, b). This would lead to the rotation of magnetic particles towards the shear plane, depending on the amount of finite strain (gamma) and particle axial ratio. In the presented example, we observe a clockwise rotation of magnetic lineation and foliation plane by 10° accompanied by a slight increase in the degree of anisotropy and a shift of the AMS ellipsoid from oblate towards the neutral and

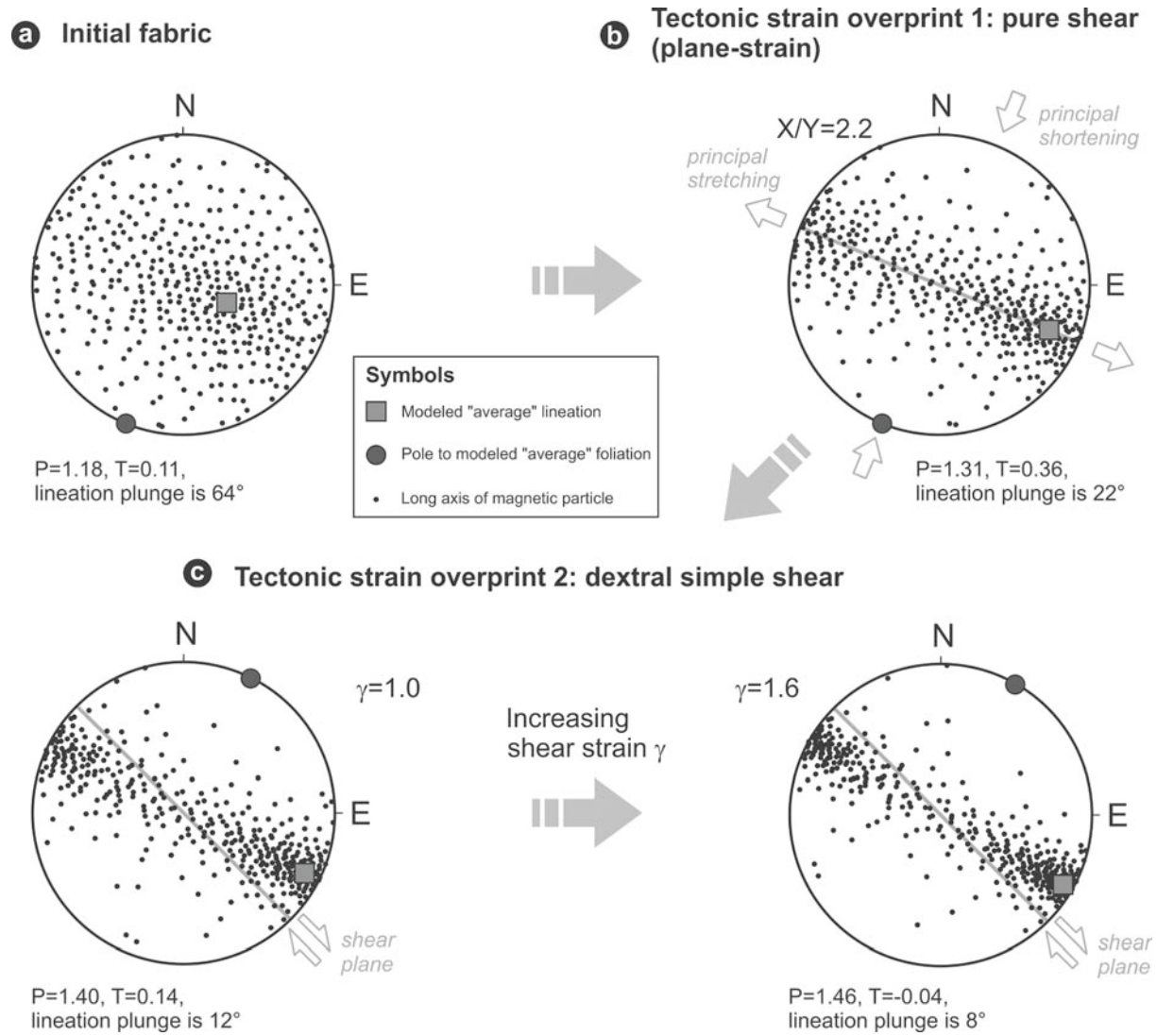

Fig. 10. Results of numerical simulations (plotted on lower hemisphere, equal area projection) showing magnetic fabric evolution (a–c) in response to tectonic pure and simple shear superposed on an earlier fabric.

prolate fields.

Our numerical modeling yielded calculated finite fabric parameters matching well the measured AMS data (Figs. 9, 10). Superposition of pure shear and then dextral simple shear on the pre-existing fabric (Fig. 10) thus seems a plausible model to explain the complex structural evolution of the Radisson pluton (Fig. 11a).

7.4. Solid-state deformation and younger intrusions

The NW–SE-trending zone of high-temperature solid-state foliation cross-cutting the western part of the pluton is also associated with a shallowly-plunging magnetic lineation (Figs. 2, 9b). This zone contains shear-band S–C fabric and winged K-feldspar porphyroclasts that indicate a regionally consistent dextral simple shear component (Fig. 3d, 4d). We suggest that this solid-state shear zone developed during the same ~NNE–SSW shortening and records strain localization as the pluton cooled (Fig. 11a).

The ca. 2697 Ma Chisasibi magma-mingling complex appears to have intruded as flat-lying or gently inclined magmatic sheets and enclave swarms (Figs. 2, 3g). The pervasive solid-state deformation is mostly absent, yet the mafic schlieren and magmatic fabric have likely been folded about the ~WNW–ESE to ~NW–SE horizontal stretching axis, plotting as pronounced girdle poles to foliation on a stereonet (Fig. 2); magnetic foliations and lineations follow the same orientation distribution (Fig. 9d). This phase thus marks the waning stage of the ~NNE–SSW compression.

Last, an undeformed felsic dike that cuts across the pervasive solid-state fabric in the Radisson pluton was dated at ca. 2696 Ma (unpublished U–Pb age; Fig. 3h). Interestingly, the late-stage felsic dikes cutting across all units strike predominantly ~NW–SE, suggesting a ~NE–SW principal extension (Fig. 2). The dike orientation, not perpendicular to subhorizontal magnetic lineations and to the inferred principal stretching direction, thus suggest they did not evolve in a kinematic continuum (e.g., Bouillin et al., 1993; Benn et al., 2001), representing a separate tectonic event after cooling and solidification of the Radisson pluton. This event still remains to be fully explored, but it may be explained as a result of post-compressional brittle relaxation along the Bienville–La Grande boundary.

7.5. Implications for the late Archean assembly of the Superior Province

The above inferences are in agreement with a general notion that syn-tectonic granitic plutons are sensitive markers of large-scale crustal strain. After magma emplacement but before final solidification, plutons are composed of crystal–melt framework and behave as weak inclusions capable of transmitting deviatoric stresses within the stiffer crust (e.g.,

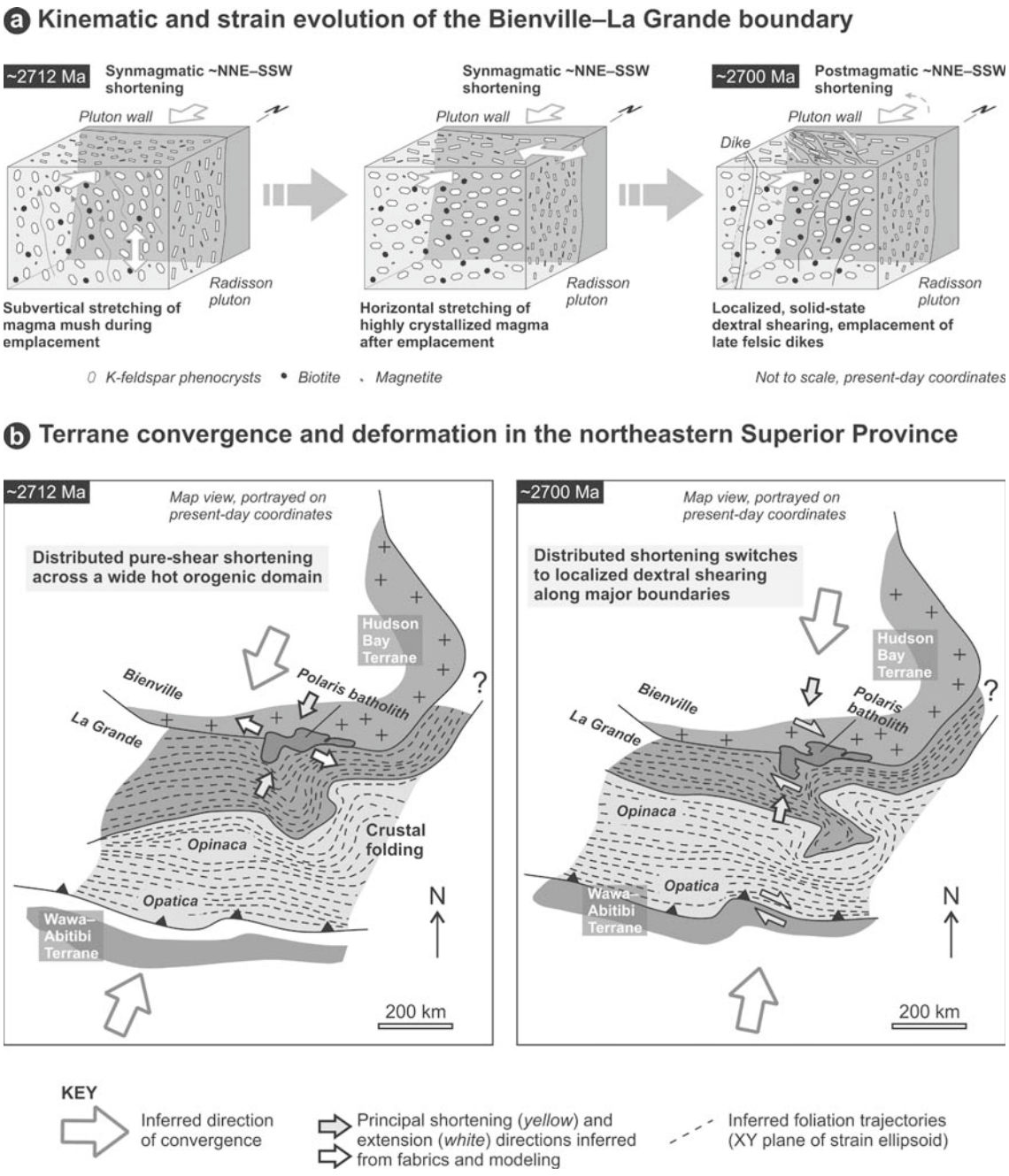

Fig. 11. Interpretive sketches to show kinematics and strain superposition recorded in the Radisson pluton and adjacent intrusive complexes as inferred from the field and AMS data and numerical modeling. (a) Block-diagrams show fabric evolution from steep lineation to horizontal lineation resulting from syn-magmatic pure shear shortening to localized solid-state dextral shears. (b) Large-scale tectonic model (map) for the two-stage Late Archean assembly of the northeastern Superior Province based on the deformation succession in the Radisson pluton and correlation with the southerly terranes (e.g., Daigneault et al., 2002; Percival et al., 2012).

Yoshinobu et al., 2009). Even small amounts of tectonic shortening (5–10 %) imposed on a crystal–melt framework cause crystals to realign, mostly by melt-aided grain-boundary sliding, with their largest faces perpendicular to principal shortening and their longest axes parallel to principal stretching (e.g., Benn, 1994; Park and Means, 1996). This applies both for K-feldspar phenocrysts and microscopic magnetite crystals in the matrix, possessing the shape magnetic anisotropy, which is the case of the plutonic units examined here. Moreover, it has been increasingly recognized that magmatic and magnetic fabric axes may not only track the principal strain axes (e.g., Benn, 2010), but also stress within the upper crust (e.g., Callahan and Markley, 2003) and plate motion vectors (e.g., Benn et al., 2001). In some of the Mesozoic Cordilleran arc plutons, the normals to magmatic foliation were interpreted as recording the direction of plate convergence during emplacement (e.g., Tikoff and de Saint Blanquat, 1997; Cao et al., 2015).

Similarly, if fabrics closely match the plate/terrane convergence direction, this approach opens an exciting possibility of evaluating the assembly of the Superior Province during the Late Archean. The models that have been proposed differ fundamentally and in some cases portray only the southwestern portion of the Province avoiding to explain the prominent curvature of lithotectonic belts in the northeast. Nevertheless, each of the models implies specific regional strain patterns and sense of shear along terrane boundaries and may thus be rigorously tested against our structural and magnetic fabric data.

Most of the published studies agreed upon attachment of the outboard ~E–W-trending terranes to the southern edge of the ‘Superior

proto-craton', progressing from north to south and implying a more or less frontal convergence and ~NNE–SSW shortening (e.g., Percival et al., 2006; Percival et al., 2012). Yet, the driving forces remain elusive as does the mechanism of orogenic curvature. Bédard (2018) invoked terrane 'subcretion' driven by mantle traction (perhaps radially from all sides of the nucleus?), as opposed to modern-style plate-tectonic scenarios driven by subduction and slab-pull force. Two models attempted to explain the orogenic curvature and thus the architecture of the Superior Province as a whole. In an earlier interpretation, Percival et al. (1994) suggested that the ~N–S-trending belts (Vizien, Utsalik) were accreted frontally while, at the same time, the ~E–W-trending terrane boundaries experienced dextral transpressional shearing. In this concept, the orogenic curvature would represent more or less a primary arc (using the terminology of Weil and Sussman, 2004). In contrast, based on a geometric similarity with some of the well-documented Phanerozoic oroclines, van der Voo (2004) speculated that the Superior Province may have formed by oroclinal bending of originally linear, or at least straighter, external belts around the proto-cratonic core.

Despite covering a small area, our structural and rock-magnetic study may add some new constraints to the above outlined tectonic models. First, we have argued that the magmatic to high-temperature solid-state fabrics along the Bienville–La Grande boundary record ~NNE–SSW shortening and simultaneous lateral stretching/extrusion (Fig. 11a). We interpret these fabrics as a signal of far-field, frontal, ~NNE-directed terrane convergence that occurred outboard of the presumed arc margin/cratonic core (Fig. 10b). Importantly, the dextral terrane-parallel shearing took place as a later phase that reactivated the Bienville–La Grande boundary at least partly in a brittle regime (Fig. 11a, b). This later phase matches remarkably the dextral transpression that was inferred to have controlled amalgamation of the outboard Abitibi greenstone belt at virtually the same time between ca. 2700 Ma and 2692 Ma (e.g., Daigneault et al., 2002). Taken together, although our structural study cannot constrain the driving forces, it strongly favors the ~NNE-directed terrane assembly of the northeastern Superior Province that was followed by localized dextral reactivation (Fig. 11). This two-phase evolution may indicate a slight anti-clockwise rotation of the plate convergence vector (Fig. 11b) while the initially hot, magma-rich crust, cooled down and became progressively rheologically 'locked' to accommodate further shortening.

Lastly, the dextral transpressive shear zones that were active simultaneously along the Hudson Bay and Wawa–Abitibi terrane margins imply not only significant horizontal stretching and shearing but also large differential stresses to be transmitted across the crustal region in between (Fig. 11b). The curved margins of the Polaris batholith and La Grande domain are suggestive of crustal folding (Figs. 1, 11b) and are compatible with this interpretation. Altogether these features are difficult to reconcile with plume-related vertical tectonics. Moreover, the general two-stage succession of events, frontal collision/accretion followed by horizontal shearing along terrane boundaries, is similar to modern accretionary plate margins and Cordilleran continental-margin arcs (e.g., McClelland et al., 2000; Cagnard et al., 2011; Moyen and Laurent, 2018) while the homogeneous deformation distributed over hundreds of kilometers wide crustal domains resembles large hot orogens such as the Variscan belt or Himalaya (e.g., Cruden et al., 2006; Chardon et al., 2009; Jamieson and Beaumont, 2013). However, to fully understand the Late Archean accretionary tectonics of the Superior Province, a detailed structural analysis is needed from the poorly accessible but crucial area where the ~N–S terrane boundaries bend around the proto-cratonic core into an ~E–W orientation (question mark in Fig. 11b). This remains an open target for future research.

8. Conclusions

The Radisson pluton intruded the boundary between the Bienville and La Grande domains of the Superior Province at around 2712 Ma. The pluton preserves a margin-parallel magmatic foliation that contains a steep lineation, recognized by the AMS, interpreted as recording vertical stretching and horizontal flattening of highly crystallized magma due to emplacement or pure shear-dominated transpression. More widespread, however, is a horizontal lineation within the same foliation that is interpreted as recording post-emplacement, but still syn-magmatic, tectonic strain. This fabric continues into the host gneisses as solid-state and, hence, overprinted the pluton–host rock system during frontal terrane collisions and simultaneous lateral extrusion (terrane-parallel stretching). Localized S–C mylonite zones accommodated further shortening upon pluton cooling. Late-stage felsic dikes cross-cut the pluton and are undeformed, yet their systematic orientation oblique to the pluton margins points to a change from frontal terrane convergence/accretion to dextral shearing. In summary, these inferences suggest a two-stage evolution of the northeastern Superior Province during the Late Archean. The NNE-directed terrane convergence and attachment to the cratonic nucleus occurred in a 'hot' regime with voluminous syn-collisional plutonism and was followed by more localized dextral shearing along terrane boundaries, perhaps caused by an anticlockwise rotation of plate convergence vector, a tectonic style that is observed in modern accretionary orogens.

CRediT authorship contribution statement

Jiří Žák: Conceptualization, Investigation, Writing – original draft, Writing – review & editing. **Filip Tomek:** Conceptualization, Investigation, Writing – original draft, Writing – review & editing. **Martin Svojtka:** Conceptualization, Investigation, Writing – original draft, Writing – review & editing. **František Vacek:** Conceptualization, Investigation, Writing – original draft, Writing – review & editing. **Václav Kachlík:** Conceptualization, Investigation, Writing – original draft, Writing – review & editing. **Lukáš Ackerman:** Conceptualization, Investigation, Writing – original draft, Writing – review & editing. **Josef Ježek:** Conceptualization, Investigation, Writing – original draft, Writing – review & editing. **Michael S. Petronis:** Conceptualization, Investigation, Writing – original draft, Writing – review & editing.

Declaration of Competing Interest

The authors declare that they have no known competing financial interests or personal relationships that could have appeared to influence the work reported in this paper.

Acknowledgements

We gratefully acknowledge the contribution of two anonymous reviewers through their very constructive and helpful reviews of the original manuscript and Victoria Pease for editorial handling. Jaroslav Dostal (Halifax) is thanked for the discussions and help with the preparation of the project, Milena Vostrá and Marta Tomková are thanked for laboratory assistance. Resto Chez Mika (Radisson) and Auberge Maanitaaukimikw (Chisasibi) are thanked for their hospitality. This study was supported by the Czech Science Foundation through Grant No. 19-08066S (to Jiří Žák), by the Charles University through projects PROGRES Q45 and Center for Geosphere Dynamics (UNCE/SCI/006), by the Institute of Geology of the Czech Academy of Sciences institutional support RVO67985831 (to Martin Svojtka and Lukáš Ackerman), and by the National Science Foundation through Grants DMR-1523611 and DMR-2122108 (PREM).

Appendix A. Supplementary data

Supplementary data to this article can be found online at https://doi.org/10.1016/j.precamres.2021.106322.

References

Archanjo, C.J., Trindade, R.I.F., Bouchez, J.L., Ernesto, M., 2002. Granite fabrics and regional-scale strain partitioning in the Seridó belt (Borborema Province, NE Brazil). Tectonics 21 (1), 3-1–3-14. https://doi.org/10.1029/2000TC001269.

Arndt, N., 2013. Formation and evolution of the continental crust. Geochem. Perspect. 2 (3), 405–533.

Bédard, J.H., 2006. A catalytic delamination-driven model for coupled genesis of Archaean crust and sub-continental lithospheric mantle. Geochim. Cosmochim. Acta 70 (5), 1188–1214.

Bédard, J.H., 2018. Stagnant lids and mantle overturns: implications for Archaean tectonics, magmagenesis, crustal growth, mantle evolution, and the start of plate tectonics. Geosci. Front. 9 (1), 19–49.

Bédard, J.H., Brouillette, P., Madore, L., Berclaz, A., 2003. Archaean cratonization and deformation in the northern Superior Province, Canada: an evaluation of plate tectonic versus vertical tectonic models. Precambr. Res. 127 (1-3), 61–87.

Bédard, J.H., Harris, L.B., 2014. Neoarchean disaggregation and reassembly of the Superior craton. Geology 42, 951–954.

Benn, K., 1994. Overprinting of magnetic fabrics in granites by small strains: numerical modeling. Tectonophysics 233, 153–162.

Benn, K., 2010. Anisotropy of magnetic susceptibility fabrics in syntectonic plutons as tectonic strain markers: the example of the Canso pluton, Meguma Terrane, Nova Scotia. Earth Environ. Sci. Trans. R. Soc. Edinburgh 100 (1-2), 147–158.

Benn, K., Ham and, N.M., Pignotta, G.S., Bleeker, W., 1998. Emplacement and deformation of granites during transpression: magnetic fabrics of the Archean Sparrow pluton, Slave Province, Canada. J. Struct. Geol. 20 (9-10), 1247–1259.

Benn, K., Paterson, S.R., Lund, S.P., Pignotta, G.S., Kruse, S., 2001. Magmatic fabrics in batholiths as markers of regional strains and plate kinematics: example of the Cretaceous Mt. Stuart batholith. Phys. Chem. Earth Part A. 26 (4-5), 343–354.

Berthé, D., Choukroune, P., Jegouzo, P., 1979. Orthogneiss, mylonite and non coaxial deformation of granites: the example of the South Armorican Shear Zone. J. Struct. Geol. 1 (1), 31–42.

Bloem, E.J.M., Dalstra, H.J., Ridley, J.R., Groves, D.I., 1997. Granitoid diapirism during protracted tectonism in an Archaean granitoid–greenstone belt, Yilgarn Block, Western Australia. Precambr. Res. 85 (3-4), 147–171.

Borradaile, G.J., Henry, B., 1997. Tectonic applications of magnetic susceptibility and its anisotropy. Earth Sci. Rev. 42 (1-2), 49–93.

Borradaile, G.J., Jackson, M., 2010. Structural geology, petrofabrics and magnetic fabrics (AMS, AARM, AIRM). J. Struct. Geol. 32 (10), 1519–1551.

Bouhallier, H., Choukroune, P., Ballèvre, M., 1993. Diapirism, bulk homogeneous shortening and transcurrent shearing in the Archaean Dharwar craton: the Holenarsipur area, southern India. Precambr. Res. 63 (1-2), 43–58.

Bouchez, J.L., 1997. Granite is never isotropic: an introduction to AMS studies of granitic rocks. In: J.L. Bouchez, D.H.W. Hutton and W.E. Stephens (Editors), Granite: From Segregation of Melt to Emplacement Fabrics. Kluwer Academic Publishers, pp. 95–112.

Bouchez, J.L., 2000. Magnetic susceptibility anisotropy and fabrics in granites. Compt. Rendus L'Acad. Sci. – Series IIA – Earth Planet. Sci. 330, 1–14.

Bouillin, J.-P., Bouchez, J.-L., Lespinasse, P., Pêcher, A., 1993. Granite emplacement in an extensional setting: an AMS study of the magmatic structures of Monte-Capanne (Elba, Italy). Earth Planet. Sci. Lett. 118 (1-4), 263–279.

Brown, M., Johnson, T., 2018. Secular change in metamorphism and the onset of global plate tectonics. Am. Mineral. 103, 181–196.

Brown, M., Johnson, T., Gardiner, N.J., 2020. Plate tectonics and the Archean Earth. Annu. Rev. Earth Planet. Sci. 48 (1), 291–320.

Brun, J.P., Gapais, D., Le Theoff, B., 1981. The mantled gneiss domes of Kuopio (Finland): interfering diapirs. Tectonophysics 74 (3-4), 283–304.

Burton-Johnson, A., Macpherson, C.G., Muraszko, J.R., Harrison, R.J., Jordan, T.A., 2019. Tectonic strain recorded by magnetic fabrics (AMS) in plutons, including Mt Kinabalu, Borneo: a tool to explore past tectonic regimes and syn-magmatic deformation. J. Struct. Geol. 119, 50–60.

Cagnard, F., Barbey, P., Gapais, D., 2011. Transition between "Archaean-type" and "modern-type" tectonics: Insights from the Finnish Lapland Granulite Belt. Precambr. Res. 187 (1-2), 127–142.

Callahan, C.N., Markley, M.J., 2003. A record of crustal-scale stress: igneous foliation and lineation in the Mount Waldo Pluton, Waldo County, Maine. J. Struct. Geol. 25 (4), 541–555.

Calvert, A.J., Ludden, J.N., 1999. Archean continental assembly in the southeastern Superior Province of Canada. Tectonics 18 (3), 412–429.

Calvert, A.J., Sawyer, E.W., Davis, W.J., Ludden, J.N., 1995. Archaean subduction inferred from seismic images of a mantle suture in the Superior Province. Nature 375 (6533), 670–674.

Cao, W., Paterson, S., Memeti, V., Mundil, R., Anderson, J.L., Schmidt, K., 2015. Tracking paleodeformation fields in the Mesozoic central Sierra Nevada arc: implications for intra-arc cyclic deformation and arc tempos. Lithosphere 7 (3), 296–320.

Card, K.D., 1990. A review of the Superior Province of the Canadian Shield, a product of Archean accretion. Precambr. Res. 48 (1-2), 99–156.

Card, K.D., Ciesielski, A., 1986. Subdivisions of the Superior Province of the Canadian Shield. Geosci. Can. 13, 5–13.

Cawood, P.A., Hawkesworth, C.J., Pisarevsky, S., Dhuime, B., Capitanio, F.A. Nebel, O., 2018. Geological archive of the onset of plate tectonics. Philos. Trans. R. Soc. A 376.

Cawood, P.A., Kröner, A., Pisarevsky, S., 2006. Precambrian plate tectonics: criteria and evidence. GSA Today 16 (7), 4–11.

Cleven, N.R., Guilmette, C., Davis, D.W., Côté-Roberge, M., 2020. Geodynamic significance of Neoarchean metasedimentary belts in the Superior Province: detrital zircon U-Pb LA-ICP-MS geochronology of the Opinaca and La Grande subprovinces. Precambr. Res. 347, 105819. https://doi.org/10.1016/j.precamres.2020.105819.

Collins, W.J., Van Kranendonk, M.J., Teyssier, C., 1998. Partial convective overturn of Archaean crust in the east Pilbara Craton, Western Australia: driving mechanisms and tectonic implications. J. Struct. Geol. 20 (9-10), 1405–1424.

Condie, K.C., 2005. TTGs and adakites: are they both slab melts? Lithos 80 (1-4), 33–44.

Condie, K.C., 2018. A planet in transition: the onset of plate tectonics on Earth between 3 and 2 Ga? Geosci. Front. 9 (1), 51–60.

Cook, F.A., Percival, J.A., Clowes, R.M., 2012. Tectonic styles in Canada: LITHOPROBE perspective on the evolution of the North American continent. Geol. Assoc. Can. Spec. Pap. 49, 467–498.

Cruden, A.R., 1990. Flow and fabric development during the diapiric rise of magma. J. Geol. 98 (5), 681–698.

Cruden, A.R., Nasseri, M.H.B., Pysklywec, R., 2006. Surface topography and internal strain variation in wide hot orogens from three-dimensional analogue and two-dimensional numerical vice models. In: Buiter, S.J.H., Schreurs, G. (Eds.), Analogue and Numerical Modelling of Crustal-Scale Processes. Geological Society, London, Special Publications, pp. 79–104.

Czarnota, K., Champion, D.C., Goscombe, B., Blewett, R.S., Cassidy, K.F., Henson, P.A., Groenewald, P.B., 2010. Geodynamics of the eastern Yilgarn Craton. Precambr. Res. 183 (2), 175–202.

Daigneault, R., Mueller, W.U., Chown, E.H., 2002. Oblique Archean subduction: accretion and exhumation of an oceanic arc during dextral transpression, Southern Volcanic Zone, Abitibi Subprovince Canada. Precambr. Res. 115 (1-4), 261–290.

Davies, G.F., 1992. On the emergence of plate tectonics. Geology 20 (11), 963. https://doi.org/10.1130/0091-7613(1992)020<0963:OTEOPT>2.3.CO;2.

Davis, D.W., Pezzutto, F., Ojakangas, R.W., 1990. The age and provenance of metasedimentary rocks in the Quetico Subprovince, Ontario, from single zircon analyses: implications for Archean sedimentation and tectonics in the Superior Province. Earth Planet. Sci. Lett. 99 (3), 195–205.

Day, R., Fuller, M., Schmidt, V.A., 1977. Hysteresis properties of titanomagnetites: grain size and composition dependence. Phys. Earth Planet. Int. 13, 260–267.

De Wit, M., Roering, C., Hart, R.J., Armstrong, R.A., de Ronde, C.E.J., Green, R.W.E., Tredoux, M., Peberdy, E., Hart, R.A., 1992. Formation of an Archean continent. Nature 357, 553–562.

de Wit, M.J., 1998. On Archean granites, greenstones, cratons and tectonics: does the evidence demand a verdict? Precambr. Res. 91 (1-2), 181–226.

Dunlop, D.J., 1973. Superparamagnetic and single domain threshold sizes in magnetite. J. Geophys. Res. 78 (11), 1780–1793.

Dunlop, D.J., 1995. Magnetism in rocks. J. Geophys. Res. 100 (B2), 2161–2174.

Dunlop, D.J., Özdemir, Ö., 1997. Rock Magnetism: Fundamentals and Frontiers. Cambridge University Press, Cambridge.

Dutton, B.J., 1997. Finite strains in transpression zones with no boundary slip. J. Struct. Geol. 19 (9), 1189–1200.

Eriksson, P.G., Banerjee, S., Nelson, D.R., Rigby, M.J., Catuneanu, O., Sarkar, S., Roberts, R.J., Ruban, D., Mtimkulu, M.N., Sunder Raju, P.V., 2009. A Kaapvaal craton debate: nucleus of an early small supercontinent or affected by an enhanced accretion event? Gondwana Res. 15 (3-4), 354–372.

Ernst, W.G., 2009. Archean plate tectonics, rise of Proterozoic supercontinentality and onset of regional, episodic stagnant-lid behavior. Gondwana Res. 15 (3-4), 243–253.

Fowler, T.K., Paterson, S.R., 1997. Timing and nature of magmatic fabrics from structural relations around stoped blocks. J. Struct. Geol. 19 (2), 209–224.

Fralick, P., Wu, J., Williams, H.R., 1992. Trench and slope basin deposits in an Archean metasedimentary belt, Superior Province, Canadian Shield. Can. J. Earth Sci. 29 (12), 2551–2557.

Gapais, D., 1989. Shear structures within deformed granites: mechanical and thermal indicators. Geology 17 (12), 1144. https://doi.org/10.1130/0091-7613(1989)017<1144:SSWDGM>2.3.CO;2.

Gerya, T., 2014. Precambrian geodynamics: concepts and models. Gondwana Res. 25 (2), 442–463.

Ghalamghash, J., Bouchez, J.L., Vosoughi-Abedini, M., Nédélec, A., 2009. The Urumieh Plutonic Complex (NW Iran): record of the geodynamic evolution of the Sanandaj-Sirjan zone during Cretaceous times – Part II: magnetic fabrics and plate tectonic reconstruction. J. Asian Earth Sci. 36 (4-5), 303–317.

Gibb, R.A., 1975. Collision tectonics in the Canadian shield? Earth Planet. Sci. Lett. 27 (3), 378–382.

Halla, J., Whitehouse, M.J., Ahmad, T., Bagai, Z., 2017. Archaean granitoids: an overview and significance from a tectonic perspective. Geol. Soc., London, Special Publications 449 (1), 1–18.

Hamilton, W.B., 1998a. Archean magmatism and deformation were not products of plate tectonics. Precambr. Res. 91 (1-2), 143–179.

Hamilton, W.B., 1998b. Archean tectonics and magmatism. Int. Geol. Rev. 40 (1), 1–39.

Hamilton, W.B., 2011. Plate tectonics began in Neoproterozoic time, and plumes from deep mantle have never operated. Lithos 123 (1-4), 1–20.

Harrison, R.J., Muraszko, J., Heslop, D., Lascu, I., Muxworthy, A.R., Roberts, A.P., 2018. An improved algorithm for unmixing first-order reversal curve diagrams using principal component analysis. Geochem. Geophys. Geosyst. 19 (5), 1595–1610.

Heider, F., Dunlop, D.J., Sugiura, N., 1987. Magnetic properties of hydrothermally recrystallized magnetite crystals. Science 236 (4806), 1287–1290.

Harrison, T.M., Schmitt, A.K., McCulloch, M.T., Lovera, O.M., 2008. Early (≥4.5 Ga) formation of terrestrial crust: Lu–Hf, δ18O, and Ti thermometry results for Hadean zircons. Earth Planet. Sci. Lett. 268, 476–486.

Hrouda, F., 1982. Magnetic anisotropy of rocks and its application in geology and geophysics. Geophysical Surveys 5 (1), 37–82.

Hrouda, F., 1994. A technique for the measurement of thermal changes of magnetic susceptibility of weakly magnetic rocks by the CS-2 apparatus and KLY-2 Kappabridge. Geophys. J. Int. 118: 604–612.
Hrouda, F., Kahan, š., 1991. The magnetic fabric relationship between sedimentary and basement nappes in the High Tatra Mountains, N. Slovakia. J. Struct. Geol. 13 (4), 431–442.
Hrouda, F., Jelínek, V. Zapletal, K., 1997. Refined technique for susceptibility resolution into ferromagnetic and paramagnetic components based on susceptibility temperature-variation measurement. Geophys. J. Int. 129: 715–719.
Hrouda, F., Táborská, Š., Schulmann, K., Ježek, J. Dolejš, D., 1999. Magnetic fabric and rheology of co-mingled magmas in the Nasavrky Plutonic Complex (E Bohemia): implications for intrusive strain and emplacement mechanism. Tectonophysics 307: 98–111.
Chardon, D., Gapais, D., Cagnard, F., 2009. Flow of ultra-hot orogens: a view from the Precambrian, clues for the Phanerozoic. Tectonophysics 477 (3-4), 105–118.
Chardon, D., Peucat, J.-J., Jayananda, M., Choukroune, P., Fanning, C.M., 2002. Archean granite-greenstone tectonics at Kolar (South India): interplay of diapirism and bulk inhomogeneous contraction during juvenile magmatic accretion. Tectonics 21 (3), 7-1–7-17.
Jamieson, R.A., Beaumont, C., 2013. On the origin of orogens. Geol. Soc. Am. Bull. 125 (11-12), 1671–1702.
Jelsma, H.A., Dirks, P.H.G.M., 2000. Tectonic evolution of a greenstone sequence in northern Zimbabwe: sequential early stacking and pluton diapirism. Tectonics 19 (1), 135–152.
Ježek, J., Hrouda, F., 2000. The relationship between the Lisle orientation tensor and the susceptibility tensor. Phys. Chem. Earth. 25 (5), 469–474.
Ježek, J., Hrouda, F., 2002. Software for modeling the magnetic anisotropy of strained rocks. Comput. Geosci. 28 (9), 1061–1068.
Johnson, T.E., Brown, M., Gardiner, N.J., Kirkland, C.L., Smithies, R.H., 2017. Earth's first stable continents did not form by subduction. Nature 543 (7644), 239–242.
Johnston, S.T., Weil, A.B., Gutierrez-Alonso, G., 2013. Oroclines: thick and thin. Geol. Soc. Am. Bull. 125 (5-6), 643–663.
Kimura, G., Ludden, J.N., Desrochers, J.-P., Hori, R., 1993. A model of ocean-crust accretion for the Superior province, Canada. Lithos 30 (3-4), 337–355.
Korenaga, J., 2013. Initiation and evolution of plate tectonics on Earth: theories and observations. Annu. Rev. Earth Planet. Sci. 41 (1), 117–151.
Kroner, A., 1985. Evolution of the Archean continental crust. Annu. Rev. Earth Planet. Sci. 13 (1), 49–74.
Laurent, O., Martin, H., Moyen, J.F., Doucelance, R., 2014. The diversity and evolution of late-Archean granitoids: evidence for the onset of "modern-style" plate tectonics between 3.0 and 2.5 Ga. Lithos 205, 208–235.
Lister, G.S., Snoke, A.W., 1984. S-C mylonites. J. Struct. Geol. 6 (6), 617–638.
Lucas, S.B., St-Onge, M.R., 1998. Geology of the Precambrian Superior and Grenville Provinces and Precambrian fossils in North America. Geological Survey of Canada, Ottawa, p. 387.
Martin, H., Moyen, J.-F., Guitreau, M., Blichert-Toft, J., Le Pennec, J.-L., 2014. Why Archaean TTG cannot be generated by MORB melting in subduction zones. Lithos 198-199, 1–13.
Martin, H., Moyen, J.-F., Rapp, R., 2010. The sanukitoid series: magmatism at the Archaean-Proterozoic transition. Earth Environ. Sci. Trans. R. Soc. Edinburgh 100 (1-2), 15–33.
Martin, H., Smithies, R.H., Rapp, R., Moyen, J.-F., Champion, D., 2005. An overview of adakite, tonalite–trondhjemite–granodiorite (TTG), and sanukitoid: relationships and some implications for crustal evolution. Lithos 79 (1-2), 1–24.
McClelland, W.C., Tikoff, B., Manduca, C.A., 2000. Two-phase evolution of accretionary margins: examples from the North American Cordillera. Tectonophysics 326 (1-2), 37–55.
Mercier-Langevin, P., Daigneault, R., Goutier, J., Dion, C., Archer, P., 2012. Geology of the Archean intrusion-hosted La-Grande-Sud Au–Cu prospect, La Grande Subprovince, James Bay Region, Québec. Econ. Geol. 107, 935–962.
Mortensen, J., Ciesielski, A., 1987. U-Pb zircon and sphene geochronology of Archean plutonic and orthogneissic rocks of the James Bay region and Bienville Domain, Quebec. Geol. Surv. Can. Pap. 87–2, 129–134.
Moyen, J.-F., 2011. The composite Archaean grey gneisses: petrological significance, and evidence for a non-unique tectonic setting for Archaean crustal growth. Lithos 123 (1-4), 21–36.
Moyen, J.-F., Laurent, O., 2018. Archaean tectonic systems: a view from igneous rocks. Lithos 302-303, 99–125.
Moyen, J.-F., Martin, H., 2012. Forty years of TTG research. Lithos 148, 312–336.
Moyen, J.-F., Martin, H., Jayananda, M., Auvray, B., 2003. Late Archaean granites: a typology based on the Dharwar Craton (India). Precambr. Res. 127 (1-3), 103–123.
Myers, J.S., 1993. Precambrian history of the West Australian Craton and adjacent orogens. Annu. Rev. Earth Planet. Sci. 21 (1), 453–485.
Palin, R.M. Santosh, M., 2021. Plate tectonics: what, where, why, and when? Gondwana Research in press.
Palin, R.M., White, R.W., Green, E.C.R., 2016. Partial melting of metabasic rocks and the generation of tonalitic–trondhjemitic–granodioritic (TTG) crust in the Archaean: constraints from phase equilibrium modelling. Precambr. Res. 287, 73–90.
Park, Y., Means, W.D., 1996. Direct observation of deformation processes in crystal mushes. J. Struct. Geol. 18 (6), 847–858.
Passchier, C.W., Simpson, C., 1986. Porphyroclast systems as kinematic indicators. J. Struct. Geol. 8 (8), 831–843.
Paterson, S.R., Fowler, T.K., Schmidt, K.L., Yoshinobu, A.S., Yuan, E.S., Miller, R.B., 1998. Interpreting magmatic fabric patterns in plutons. Lithos 44 (1-2), 53–82.
Paterson, S.R., Miller, R.B., 1998. Stoped blocks in plutons: paleo-plumb bobs, viscometers, or chronometers? J. Struct. Geol. 20 (9-10), 1261–1272.
Paterson, S.R., Vernon, R.H., 1995. Bursting the bubble of ballooning plutons: a return to nested diapirs emplaced by multiple processes. Geol. Soc. Am. Bull. 107, 1356–1380.
Paterson, S.R., Vernon, R.H., Tobisch, O.T., 1989. A review of criteria for identification of magmatic and tectonic foliations in granitoids. J. Struct. Geol. 11, 349–363.
Pawley, M.J., Collins, W.J., Van Kranendonk, M.J., 2002. Origin of fine-scale sheeted granites by incremental injection of magma into active shear zones: examples from the Pilbara Craton, NW Australia. Lithos 61 (3-4), 127–139.
Percival, J.A., 1989. A regional perspective of the Quetico metasedimentary belt, Superior Province, Canada. Can. J. Earth Sci. 26 (4), 677–693.
Percival, J.A., 2007. Geology and metallogeny of the Superior Province, Canada. In: W.D. Goodfellow (Editor), Mineral Deposits of Canada: A Synthesis of Major Deposit-Types, District Metallogeny, the Evolution of Geological Provinces, and Exploration Methods. Geological Association of Canada, pp. 903–928.
Percival, J.A., Sanborn-Barrie, M., Skulski, T., Stott, G.M., Helmstaedt, H., White, D.J., 2006. Tectonic evolution of the western Superior Province from NATMAP and Lithoprobe studies. Can. J. Earth Sci. 43 (7), 1085–1117.
Percival, J.A., Skulski, T., Sanborn-Barrie, M., Stott, G.M., Leclair, A.D., Corkery, M.T., Boily, M., 2012. Geology and tectonic evolution of the Superior Province, Canada. Geol. Assoc. Can. Spec. Pap. 49, 321–378.
Percival, J.A., Stern, R.A., Skulski, T., 2001. Crustal growth through successive arc magmatism: reconnaissance U-Pb SHRIMP data from the northeastern Superior Province, Canada. Precambr. Res. 109 (3-4), 203–238.
Percival, J.A., Stern, R.A., Skulski, T., Card, K.D., Mortensen, J.K., Bégin, N.J., 1994. Minto block, Superior province: missing link in deciphering assembly of the craton at 2.7 Ga. Geology 22 (9), 839. https://doi.org/10.1130/0091-7613(1994)022<0839:MBSPML>2.3.CO;2.
Pike, C.R., Roberts, A.P., Dekkers, M.J., Verosub, K.L., 2001. An investigation of multi-domain hysteresis mechanisms using FORC diagrams. Phys. Earth Planet. Inter. 126 (1-2), 11–25.
Polat, A., Kerrich, R., 1999. Formation of an Archean tectonic mélange in the Schreiber-Hemlo greenstone belt, Superior Province, Canada: implications for Archean subduction–accretion process. Tectonics 18 (5), 733–755.
Polat, A., Kerrich, R., Wyman, D.A., 1998. The late Archean Schreiber-Hemlo and White River-Dayohessarah greenstone belts, Superior Province: collages of oceanic plateuaus, oceanic arcs and subduction-accretion complexes. Tectonophysics 289, 295–326.
Potter, D.K., Stephenson, A., 1988. Single-domain particles in rocks and magnetic fabric analysis. Geophys. Res. Lett. 15 (10), 1097–1100.
Ramsay, J.G., 1989. Emplacement kinematics of a granite diapir: the Chindamora batholith, Zimbabwe. J. Struct. Geol. 11 (1-2), 191–209.
Rehm, A.G., Jørgensen, T.R.C., Thurston, P.C., Gibson, H.L., Lafrance, B., 2021. Synsedimentary rifting and basaltic-komatiitic volcanism in the Pontiac subprovince, Superior craton (Canada): implications for Neoarchean geodynamics. Precambr. Res. 106204. https://doi.org/10.1016/j.precamres.2021.106204.
Roberts, A.P., Pike, C.R., Verosub, K.L., 2000. First-order reversal curve diagrams: a new tool for characterizing the magnetic properties of natural samples. J. Geophys. Res. Solid Earth 105 (B12), 28461–28475.
Roberts, A.P., Almeida, T.P., Church, N.S., Harrison, R.J., Heslop, D., Li, Y., Li, J., Muxworthy, A.R., Williams, W., Zhao, X., 2017. Resolving the origin of pseudo-single domain magnetic behavior. J. Geophys. Res. 122 (12), 9534–9558.
Sanderson, D.J., Marchini, W.R.D., 1984. Transpression. J. Struct. Geol. 6 (5), 449–458.
Sawyer, E.W., Benn, K., 1993. Structure of the high-grade Opatica Belt and adjacent low-grade Abitibi Subprovince, Canada: an Archaean mountain front. J. Struct. Geol. 15 (12), 1443–1458.
Schulmann, K., Thompson, A.B., Lexa, O., Ježek, J., 2003. Strain distribution and fabric development modeled in active and ancient transpressive zones. Journal of Geophysical Research-Solid. Earth 108 (B1), ETG 6-1–ETG 6-15.
Sleep, N.H., 1992. Archean plate tectonics: what can be learned from continental geology? Can. J. Earth Sci. 29 (10), 2066–2071.
Smithies, R.H., 2000. The Archaean tonalite–trondhjemite–granodiorite (TTG) series is not an analogue of Cenozoic adakite. Earth Planet. Sci. Lett. 182 (1), 115–125.
Smithies, R.H., Champion, D.C., Van Kranendonk, M.J., 2009. Formation of Paleoarchean continental crust through infracrustal melting of enriched basalt. Earth Planet. Sci. Lett. 281 (3-4), 298–306.
Smithies, R.H., Van Kranendonk, M.J., Champion, D.C., 2007. The Mesoarchean emergence of modern-style subduction. Gondwana Res. 11 (1-2), 50–68.
Stern, R., 2020. The Mesoproterozoic single-lid tectonic episode: prelude to modern plate tectonics. GSA Today 30 (12), 4–10.
Stem, R.A., Percival, J.A., Mortensen, J.K., 1994. Geochemical evolution of the Minto block: a 2.7 Ga continental magmatic arc built on the Superior proto-craton. Precambr. Res. 65 (1-4), 115–153.
Stern, R.J., 2008. Modern/style plate tectonics began in Neoproterozoic time: an alternative interpretation of Earth́s tectonic history. Geol. Soc. Am. Spec. Pap. 440, 265–280.
Studýnka, J., Chadima, M., Suza, P., 2014. Fully automated measurement of anisotropy of magnetic susceptibility using 3D rotator. Tectonophysics 629, 6–13.
Tarling, D.H., Hrouda, F., 1993. The Magnetic Anisotropy of Rocks. Chapman and Hall, London.
Teyssier, C., Tikoff, B., 1999. Fabric stability in oblique convergence and divergence. J. Struct. Geol. 21 (8-9), 969–974.
Tikoff, B., de Saint Blanquat, M., 1997. Transpressional shearing and strike-slip partitioning in the Late Cretaceous Sierra Nevada magmatic arc, California. Tectonics 16 (3), 442–459.
Tikoff, B., Greene, D., 1997. Stretching lineations in transpressional shear zones: an example from the Sierra Nevada Batholith, California. J. Struct. Geol. 19 (1), 29–39.

Tomek, F., Žák, J., Verner, K., Holub, F.V., Sláma, J., Paterson, S.R., Memeti, V., 2017. Mineral fabrics in high-level intrusions recording crustal strain and volcano-tectonic interactions: the Shellenbarger pluton, Sierra Nevada, California. J. Geol. Soc. 174 (2), 193–208.

van der Voo, R., 2004. Paleomagnetism, oroclines, and growth of the continental crust. GSA Today 14, 4–9.

van Hunen, J., Moyen, J.-F., 2012. Archean subduction: fact or fiction? Annu. Rev. Earth Planet. Sci. 40 (1), 195–219.

Van Kranendonk, M.J., Hugh Smithies, R., Hickman, A.H., Champion, D.C., 2007. Review: secular tectonic evolution of Archean continental crust: interplay between horizontal and vertical processes in the formation of the Pilbara Craton, Australia. Terra Nova 19 (1), 1–38.

Vernon, R.H., 2000. Review of microstructural evidence of magmatic and solid-state flow. Electronic Geosciences 5 (2), 1–23.

Weil, A.B., Sussman, A.J., 2004. Classifying curved orogens based on timing relationships between structural development and vertical-axis rotations. Geol. Soc. Am. Spec. Pap. 383, 1–15.

Whitmeyer, S.J., Karlstrom, K.E., 2007. Tectonic model for the Proterozoic growth of North America. Geosphere 3, 220–259.

Williams, H.R., 1990. Subprovince accretion tectonics in the south-central Superior Province. Can. J. Earth Sci. 27 (4), 570–581.

Windley, B.F., Kusky, T., Polat, A., 2021. Onset of plate tectonics by the Eoarchean. Precambr. Res. 352, 105980. https://doi.org/10.1016/j.precamres.2020.105980.

Wyman, D., 2018. Do cratons preserve evidence of stagnant lid tectonics? Geosci. Front. 9 (1), 3–17.

Wyman, D.A., 2013. A critical assessment of Neoarchean "plume only" geodynamics: evidence from the Superior Province. Precambr. Res. 229, 3–19.

Wyman, D.A., Kerrich, R., Polat, A., 2002. Assembly of Archean cratonic mantle lithosphere and crust: plume-arc interaction in the Abitibi-Wawa subduction-accretion complex. Precambr. Res. 115 (1-4), 37–62.

Xia, B., Zhang, L., Du, Z., Xu, B., 2019. Petrology and age of Precambrian Aksu blueschist, NW China. Precambr. Res. 326, 295–311.

Yoshinobu, A.S., Wolak, J.M., Paterson, S.R., Pignotta, G.S. Anderson, H.S., 2009. Determining relative magma and host rock xenolith rheology during magmatic fabric formation in plutons: Examples from the middle and upper crust. Geosphere 5: 270–285.

Zibra, I., 2020. Neoarchean structural evolution of the Murchison Domain (Yilgarn Craton). Precambr. Res. 343, 105719. https://doi.org/10.1016/j.precamres.2020.105719.

Žák, J., Kabele, P., 2012. A new approach to modeling perpendicular fabrics in porphyritic plutonic rocks using the finite element method. Int. J. Earth Sci. 101 (3), 715–730.

Žák, J., Verner, K., Tomek, F., Holub, F.V., Johnson, K., Schwartz, J.J., 2015. Simultaneous batholith emplacement, terrane/continent collision, and oroclinal bending in the Blue Mountains Province, North American Cordillera. Tectonics 34 (6), 1107–1128.

Žák, J., Verner, K., Tomek, F., Johnson, K., Schwartz, J.J., 2017. Magnetic fabrics of arc plutons reveal a significant Late Jurassic to Early Cretaceous change in the relative plate motions of the Pacific Ocean basin and North America. Geosphere 13 (1), 11–21.

Žák, J., Verner, K., Týcová, P., 2008. Multiple magmatic fabrics in plutons: an overlooked tool for exploring interactions between magmatic processes and regional deformation? Geol. Mag. 145 (4), 537–551.